

An adaptive finite element method in reconstruction of coefficients in Maxwell's equations from limited observations

L. Beilina^{*} S. Hosseinzadegan[†]

Abstract

We propose an adaptive finite element method for the solution of a coefficient inverse problem of simultaneous reconstruction of the dielectric permittivity and magnetic permeability functions in the Maxwell's system using limited boundary observations of the electric field in 3D.

We derive a posteriori error estimates in the Tikhonov functional to be minimized and in the regularized solution of this functional, as well as formulate corresponding adaptive algorithm. Our numerical experiments justify the efficiency of our a posteriori estimates and show significant improvement of the reconstructions obtained on locally adaptively refined meshes.

1 Introduction

This work is a continuation of the recent paper [6] and is focused on the numerical reconstruction of the dielectric permittivity $\varepsilon(x)$ and the magnetic permeability $\mu(x)$ functions in the Maxwell's system on locally refined meshes using an adaptive finite element method. The reconstruction is performed via minimization of the corresponding Tikhonov functional from backscattered single measurement data of the electric field $E(x, t)$. That means that we use backscattered boundary measurements of the wave field $E(x, t)$ which are generated by a single direction of a plane wave. In the minimization procedure we use domain decomposition finite element/finite difference methods of [4] for the numerical reconstructions of both functions.

^{*}Department of Mathematical Sciences, Chalmers University of Technology and Gothenburg University, SE-42196 Gothenburg, Sweden, e-mail: larisa@chalmers.se

[†]Department of Mathematical Sciences, Chalmers University of Technology and Gothenburg University, SE-42196 Gothenburg, Sweden, e-mail: samarh@student.chalmers.se

Comparing with [6] we present following new points here: we adopt results of [9, 10, 29] to show that the minimizer of the Tikhonov functional is closer to the exact solution than guess of this solution. We present relaxation property for the mesh refinements for the case of our inverse problem and we derive a posteriori error estimates for the error in the minimization functional and in the reconstructed functions $\varepsilon(x)$ and $\mu(x)$. Further, we formulate two adaptive algorithms and apply them in the reconstruction of small inclusions. Moreover, in our numerical simulations of this work we induce inhomogeneous initial conditions in the Maxwell's system. Non-zero initial conditions involve uniqueness and stability results of reconstruction of both unknown functions $\varepsilon(x)$ and $\mu(x)$, see details in [6, 12].

Using our numerical simulations we can conclude that an adaptive finite element method can significantly improve reconstructions obtained on a coarse non-refined mesh in order to accurately obtain shapes, locations and values of functions $\varepsilon(x)$ and $\mu(x)$.

An outline of this paper is as follows: in Section 2 we present our mathematical model and in Section 3 we formulate forward and inverse problems. In Section 4 we present the Tikhonov functional to be minimized and in Section 5 we show different versions of finite element method used in computations. In Section 6 we formulate relaxation property of mesh refinements and in Section 7 we investigate general framework of a posteriori error estimates in coefficient inverse problems (CIPs). In Sections 8, 9 we present theorems for a posteriori errors in the regularized solution of the Tikhonov functional and in the Tikhonov functional, correspondingly. In Sections 10, 11 we describe mesh refinement recommendations and formulate adaptive algorithms used in computations. Finally, in Section 12 we present our reconstruction results.

2 The mathematical model

Let a bounded domain $\Omega \subset \mathbb{R}^d$, $d = 2, 3$, have Lipschitz boundary $\partial\Omega$ and let us set $\Omega_T := \Omega \times (0, T)$, $\partial\Omega_T := \partial\Omega \times (0, T)$, where $T > 0$. We consider Maxwell's equations in an inhomogeneous isotropic media in a bounded domain $\Omega \subset \mathbb{R}^3$

$$\left\{ \begin{array}{ll} \partial_t D - \nabla \times H(x, t) = 0 & \text{in } \Omega_T \\ \partial_t B + \nabla \times E(x, t) = 0 & \text{in } \Omega_T, \\ D(x, t) = \varepsilon E(x, t), \quad B(x, t) = \mu H(x, t), & \\ E(x, 0) = E_0(x), \quad H(x, 0) = H_0(x), & \\ \nabla \cdot D(x, t) = 0, \quad \nabla \cdot B(x, t) = 0 & \text{in } \Omega_T, \\ n \times D(x, t) = 0, \quad n \cdot B(x, t) = 0 & \text{on } \partial\Omega_T, \end{array} \right. \quad (1)$$

where $x = (x_1, x_2, x_3)$. Here, $E(x, t)$ is the electric field and $H(x, t)$ is the magnetic field, $\varepsilon(x) > 0$ and $\mu(x) > 0$ are the dielectric permittivity and the magnetic

permeability functions, respectively. $E_0(x)$ and $H_0(x)$ are given initial conditions. Next, $n = n(x)$ is the unit outward normal vector to $\partial\Omega$. The electric field $E(x, t)$ is combined with the electric induction $D(x, t)$ via

$$D(x, t) = \varepsilon E(x, t) = \varepsilon_{\text{vac}} \varepsilon_r E(x, t),$$

where $\varepsilon_{\text{vac}} \approx 8.854 \times 10^{-12}$ is the vacuum permittivity which is measured in Farads per meter, and thus ε_r is the dimensionless relative permittivity. The magnetic field $H(x, t)$ is combined with the magnetic induction $B(x, t)$ via

$$B(x, t) = \mu H(x, t) = \mu_{\text{vac}} \mu_r H(x, t),$$

where $\mu_{\text{vac}} \approx 1.257 \times 10^{-6}$ is the vacuum permeability measured in Henries per meter, from what follows that μ_r is the dimensionless relative permeability.

By eliminating B and D from (1) we obtain the model problem for the electric field E with the perfectly conducting boundary conditions which is as follows:

$$\varepsilon \frac{\partial^2 E}{\partial t^2} + \nabla \times (\mu^{-1} \nabla \times E) = 0 \text{ in } \Omega_T, \quad (2)$$

$$\nabla \cdot (\varepsilon E) = 0 \text{ in } \Omega_T, \quad (3)$$

$$E(x, 0) = f_0(x), \quad E_t(x, 0) = f_1(x) \text{ in } \Omega, \quad (4)$$

$$E \times n = 0 \text{ on } \partial\Omega_T. \quad (5)$$

Here we assume that

$$f_0 \in H^1(\Omega), f_1 \in L^2(\Omega).$$

By this notation we shall mean that every component of the vector functions f_0 and f_1 belongs to these spaces. Note that equations similar to (2)-(5) can be derived also for the magnetic field H .

As in our recent work [6], for the discretization of the Maxwell's equations we use a stabilized domain decomposition method of [5]. In our numerical simulations we assume that the relative permittivity ε_r and relative permeability μ_r does not vary much which is the case of real applications, see recent experimental work [7] for similar observations. We do not impose smoothness assumptions on the coefficients $\varepsilon(x), \mu(x)$ and we treat discontinuities in a similar way as in [17]. Thus, a discontinuous finite element method should be applied for the finite element discretization of these functions, see details in Section 5.

3 Statements of forward and inverse problems

We divide Ω into two subregions, Ω_{FEM} and Ω_{OUT} such that $\bar{\Omega} = \bar{\Omega}_{\text{FEM}} \cup \bar{\Omega}_{\text{OUT}}$, $\Omega_{\text{FEM}} \cap \Omega_{\text{OUT}} = \emptyset$ and $\partial\Omega_{\text{FEM}} \subset \partial\Omega_{\text{OUT}}$. For an illustration of the domain

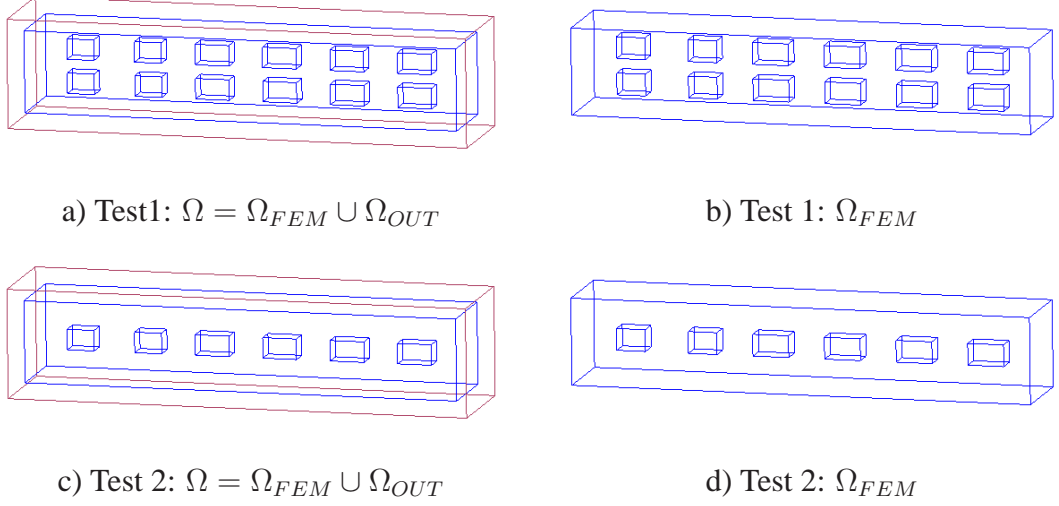


Figure 1: Domain decomposition in numerical tests of Section 12. a), c) The decomposed domain $\Omega = \Omega_{FEM} \cup \Omega_{OUT}$. b), d) The finite element domain Ω_{FEM} .

decomposition, see Figure 1. The boundary $\partial\Omega$ is such that $\partial\Omega = \partial_1\Omega \cup \partial_2\Omega \cup \partial_3\Omega$ where $\partial_1\Omega$ and $\partial_2\Omega$ are, respectively, front and back sides of the domain Ω , and $\partial_3\Omega$ is the union of left, right, top and bottom faces of this domain. For numerical solution of (2)-(5) in Ω_{OUT} we can use either the finite difference or the finite element method on a structured mesh with constant coefficients $\varepsilon = 1$ and $\mu = 1$. In Ω_{FEM} , we use finite elements on a sequence of unstructured meshes $K_h = \{K\}$, with elements K consisting of triangles in \mathbb{R}^2 and tetrahedra in \mathbb{R}^3 satisfying the maximal angle condition [15]. Let $S_T := \partial_1\Omega \times (0, T)$ where $\partial_1\Omega$ is the backscattering side of the domain Ω with the time domain observations, and define by $S_{1,1} := \partial_1\Omega \times (0, t_1]$, $S_{1,2} := \partial_1\Omega \times (t_1, T)$, $S_2 := \partial_2\Omega \times (0, T)$, $S_3 := \partial_3\Omega \times (0, T)$.

To simplify notations, further we will omit subscript r in ε_r and μ_r . We add a Coulomb-type gauge condition [1, 31] to (2)-(5) for stabilization of the finite element solution using the standard piecewise continuous functions with $0 \leq s \leq$

1, and our model problem (2)-(5) which we use in computations rewrites as

$$\begin{aligned}
\varepsilon \frac{\partial^2 E}{\partial t^2} + \nabla \times (\mu^{-1} \nabla \times E) - s \nabla (\nabla \cdot (\varepsilon E)) &= 0 \text{ in } \Omega_T, \\
E(x, 0) = f_0(x), \quad E_t(x, 0) = f_1(x) &\text{ in } \Omega, \\
\partial_n E &= (0, f(t), 0) \text{ on } S_{1,1}, \\
\partial_n E &= -\partial_t E \text{ on } S_{1,2}, \\
\partial_n E &= -\partial_t E \text{ on } S_2, \\
\partial_n E &= 0 \text{ on } S_3, \\
\mu(x) = \varepsilon(x) = 1 &\text{ in } \Omega_{\text{OUT}}.
\end{aligned} \tag{6}$$

In the recent works [4, 6, 7] was demonstrated numerically that the solution of the problem (6) approximates well the solution of the original Maxwell's system for the case when $1 \leq \mu(x) \leq 2$, $1 \leq \varepsilon(x) \leq 15$ and $s = 1$.

We assume that our coefficients $\varepsilon(x)$, $\mu(x)$ of equation (6) are such that

$$\begin{aligned}
\varepsilon(x) &\in [1, d_1], \quad d_1 = \text{const.} > 1, \quad \varepsilon(x) = 1 \text{ for } x \in \Omega_{\text{OUT}}, \\
\mu(x) &\in [1, d_2], \quad d_2 = \text{const.} > 1, \quad \mu(x) = 1 \text{ for } x \in \Omega_{\text{OUT}}, \\
\varepsilon(x), \mu(x) &\in C^2(\mathbb{R}^3).
\end{aligned} \tag{7}$$

In our numerical tests the values of constants d_1, d_2 in (7) are chosen from experimental set-up similarly with [7, 36] and we assume that we know them a priori.

This is in agreement with the availability of a priori information for an ill-posed problem [2, 21, 38]. Through the work we use following notations: for any vector function $u \in \mathbb{R}^3$ when we write $u \in H^k(\Omega)$, $k = 1, 2$, we mean that every component of the vector function u belongs to this space. We consider the following

Inverse Problem (IP) *Assume that the functions $\varepsilon(x)$ and $\mu(x)$ satisfy conditions (7) for the known $d_1, d_2 > 1$ and they are unknown in the domain $\Omega \setminus \Omega_{\text{OUT}}$. Determine the functions $\varepsilon(x)$, $\mu(x)$ for $x \in \Omega \setminus \Omega_{\text{OUT}}$, assuming that the following function $\tilde{E}(x, t)$ is known*

$$E(x, t) = \tilde{E}(x, t) \quad \forall (x, t) \in S_T. \tag{8}$$

The function $\tilde{E}(x, t)$ in (8) represents the time-dependent measurements of the electric wave field $E(x, t)$ at the backscattering boundary $\partial_1 \Omega$. In real-life experiments, measurements are performed on a number of detectors, see details in our recent experimental work [7].

4 Tikhonov functional

We reformulate our inverse problem as an optimization problem, where we seek for two functions, the permittivity $\varepsilon(x)$ and permeability $\mu(x)$, which result in a solution of equations (6) with best fit to time and space domain observations \tilde{E} , measured at a finite number of observation points on $\partial_1\Omega$. Our goal is to minimize the Tikhonov functional

$$\begin{aligned} J(\varepsilon, \mu) := J(E, \varepsilon, \mu) &= \frac{1}{2} \int_{S_T} (E - \tilde{E})^2 z_\delta(t) d\sigma dt \\ &+ \frac{1}{2} \gamma_1 \int_{\Omega} (\varepsilon - \varepsilon_0)^2 dx + \frac{1}{2} \gamma_2 \int_{\Omega} (\mu - \mu_0)^2 dx, \end{aligned} \quad (9)$$

where \tilde{E} is the observed electric field, E satisfies the equations (6) and thus depends on ε and μ , ε_0 is the initial guess for ε and μ_0 is the initial guess for μ , and $\gamma_i, i = 1, 2$ are the regularization parameters. Here, $z_\delta(t)$ is a cut-off function, which is introduced to ensure that the compatibility conditions at $\overline{\Omega_T} \cap \{t = T\}$ for the adjoint problem (18) are satisfied, and $\delta > 0$ is a small number. The function z_δ can be chosen as in [6].

Next, we introduce the following spaces of real valued vector functions

$$\begin{aligned} H_E^1 &:= \{w \in H^1(\Omega_T) : w(\cdot, 0) = 0\}, \\ H_\lambda^1 &:= \{w \in H^1(\Omega_T) : w(\cdot, T) = 0\}, \\ U^1 &= H_E^1(\Omega_T) \times H_\lambda^1(\Omega_T) \times C(\overline{\Omega}) \times C(\overline{\Omega}), \\ U^0 &= L_2(\Omega_T) \times L_2(\Omega_T) \times L_2(\Omega) \times L_2(\Omega). \end{aligned} \quad (10)$$

We also define the L_2 inner product and the norm over Ω_T and Ω as

$$\begin{aligned} ((u, v))_{\Omega_T} &= \int_{\Omega} \int_0^T uv dx dt, \\ ||u||^2 &= ((u, u))_{\Omega_T}, \\ (u, v)_{\Omega} &= \int_{\Omega} uv dx, \\ |u|^2 &= (u, u)_{\Omega}. \end{aligned}$$

To solve the minimization problem we take into account (7) and introduce the Lagrangian

$$\begin{aligned} L(u) &= J(E, \varepsilon, \mu) - ((\varepsilon \partial_t \lambda, \partial_t E))_{\Omega_T} - (\varepsilon \lambda(x, 0), f_1(x))_{\Omega} + ((\mu^{-1} \nabla \times E, \nabla \times \lambda))_{\Omega_T} \\ &+ s ((\nabla \cdot (\varepsilon E), \nabla \cdot \lambda))_{\Omega_T} - ((\lambda, p(t)))_{S_{1,1}} + ((\lambda \partial_t E))_{S_{1,2}} + ((\lambda \partial_t E))_{S_2}, \end{aligned} \quad (11)$$

where $u = (E, \lambda, \varepsilon, \mu) \in U^1$ and $p(t) = (0, f(t), 0)$ and ∂_t define the derivative in time. We now search for a stationary point of the Lagrangian with respect to u satisfying for all $\bar{u} = (\bar{E}, \bar{\lambda}, \bar{\varepsilon}, \bar{\mu}) \in U^1$

$$L'(u; \bar{u}) = 0, \quad (12)$$

where $L'(u; \cdot)$ is the Jacobian of L at u . Equation above can be written as

$$L'(u; \bar{u}) = \frac{\partial L}{\partial \lambda}(u)(\bar{\lambda}) + \frac{\partial L}{\partial E}(u)(\bar{E}) + \frac{\partial L}{\partial \varepsilon}(u)(\bar{\varepsilon}) + \frac{\partial L}{\partial \mu}(u)(\bar{\mu}) = 0. \quad (13)$$

To find the Frechét derivative (13) of the Lagrangian (11) we consider $L(u + \bar{u}) - L(u)$ for all $\bar{u} \in U^1$ and single out the linear part of the obtained expression with respect to \bar{u} . In our derivation of the Frechét derivative we assume that in the Lagrangian (11) functions $u = (E, \lambda, \varepsilon, \mu) \in U^1$ can vary independently of each other. In this approach we obtain the same result as by assuming that functions E and λ are dependent on the coefficients ε, μ , see also Chapter 4 of [9] where similar observations take place. Taking into account that $E(x, t)$ is the solution of the forward problem (6), assumptions that $\lambda(x, T) = \frac{\partial \lambda}{\partial t}(x, T) = 0$, as well as $\mu = \varepsilon = 1$ on $\partial\Omega$ and using conditions (7), we obtain from (13) that for all \bar{u} ,

$$\begin{aligned} 0 = \frac{\partial L}{\partial \lambda}(u)(\bar{\lambda}) &= -((\varepsilon \partial_t \bar{\lambda}, \partial_t E))_{\Omega_T} - (\varepsilon f_1(x), \bar{\lambda}(x, 0))_{\Omega} + ((\mu^{-1} \nabla \times E, \nabla \times \bar{\lambda}))_{\Omega_T} \\ &\quad + s((\nabla \cdot (\varepsilon E), \nabla \cdot \bar{\lambda}))_{\Omega_T} - ((\bar{\lambda}, p(t)))_{S_{1,1}} + ((\bar{\lambda}, \partial_t E))_{S_{1,2}} \\ &\quad + ((\bar{\lambda}, \partial_t E))_{S_2} \quad \forall \bar{\lambda} \in H_{\lambda}^1(\Omega_T), \end{aligned} \quad (14)$$

$$\begin{aligned} 0 = \frac{\partial L}{\partial E}(u)(\bar{E}) &= ((E - \tilde{E}, \bar{E} z_{\delta}))_{S_T} - ((\varepsilon \partial_t \lambda, \partial_t \bar{E}))_{\Omega_T} + ((\mu^{-1} \nabla \times \lambda, \nabla \times \bar{E}))_{\Omega_T} \\ &\quad + s((\nabla \cdot \lambda, \nabla \cdot (\varepsilon \bar{E}))_{\Omega_T} - ((\partial_t \lambda, \bar{E}))_{S_{1,2} \cup S_2} - (\varepsilon \bar{E}(x, 0), \partial_t \lambda(x, 0))) \quad \forall \bar{E} \in H_E^1(\Omega_T). \end{aligned} \quad (15)$$

Further, we obtain two equations that express that the gradients with respect to ε and μ vanish:

$$\begin{aligned} 0 = \frac{\partial L}{\partial \varepsilon}(u)(\bar{\varepsilon}) &= -((\partial_t \lambda, \partial_t E \bar{\varepsilon}))_{\Omega_T} - (\lambda(x, 0), f_1(x) \bar{\varepsilon})_{\Omega} \\ &\quad + s((\nabla \cdot (\bar{\varepsilon} E), \nabla \cdot \lambda))_{\Omega_T} + \gamma_1(\varepsilon - \varepsilon_0, \bar{\varepsilon})_{\Omega} \quad \forall x \in \Omega, \end{aligned} \quad (16)$$

$$0 = \frac{\partial L}{\partial \mu}(u)(\bar{\mu}) = -((\mu^{-2} \nabla \times E, \nabla \times \lambda \bar{\mu}))_{\Omega_T} + \gamma_2(\mu - \mu_0, \bar{\mu})_{\Omega} \quad \forall x \in \Omega. \quad (17)$$

We observe that the equation (14) is the weak formulation of the state equation (6) and the equation (15) is the weak formulation of the following adjoint problem

$$\begin{aligned}
\varepsilon \frac{\partial^2 \lambda}{\partial t^2} + \nabla \times (\mu^{-1} \nabla \times \lambda) - s\varepsilon \nabla (\nabla \cdot \lambda) &= -(E - \tilde{E})|_{S_T z_\delta} \text{ in } \Omega_T, \\
\lambda(\cdot, T) = \frac{\partial \lambda}{\partial t}(\cdot, T) &= 0, \\
\partial_n \lambda &= \partial_t \lambda \text{ on } S_{1,2}, \\
\partial_n \lambda &= \partial_t \lambda \text{ on } S_2, \\
\partial_n \lambda &= 0 \text{ on } S_3,
\end{aligned} \tag{18}$$

which is solved backward in time.

We now define by $E(\varepsilon, \mu)$, $\lambda(\varepsilon, \mu)$ the exact solutions of the forward and adjoint problems for given ε, μ , respectively. Then defining by

$$u(\varepsilon, \mu) = (E(\varepsilon, \mu), \lambda(\varepsilon, \mu), \varepsilon, \mu) \in U^1,$$

using the fact that for exact solutions $E(\varepsilon, \mu)$, $\lambda(\varepsilon, \mu)$ because of (11) we have

$$J(E(\varepsilon, \mu), \varepsilon, \mu) = L(u(\varepsilon, \mu)), \tag{19}$$

and assuming that solutions $E(\varepsilon, \mu)$, $\lambda(\varepsilon, \mu)$ are sufficiently stable, see Chapter 5 of book [30] for details, we can write that the Frechét derivative of the Tikhonov functional is the function $J'(\varepsilon, \mu, E(\varepsilon, \mu))$ which is defined as

$$\begin{aligned}
J'(\varepsilon, \mu) &:= J'(\varepsilon, \mu, E(\varepsilon, \mu)) = \frac{\partial J}{\partial \varepsilon}(\varepsilon, \mu, E(\varepsilon, \mu)) + \frac{\partial J}{\partial \mu}(\varepsilon, \mu, E(\varepsilon, \mu)) \\
&= \frac{\partial L}{\partial \varepsilon}(u(\varepsilon, \mu)) + \frac{\partial L}{\partial \mu}(u(\varepsilon, \mu)).
\end{aligned} \tag{20}$$

Inserting (16) and (17) into (20), we get

$$\begin{aligned}
J'(\varepsilon, \mu)(x) &:= J'(\varepsilon, \mu, E(\varepsilon, \mu))(x) = - \int_0^T \partial_t \lambda \partial_t E(x, t) dt - \lambda(x, 0) f_1(x) \\
&\quad + s \int_0^T (\nabla \cdot E)(\nabla \cdot \lambda)(x, t) dt + \gamma_1(\varepsilon - \varepsilon_0)(x) \\
&\quad - \int_0^T (\mu^{-2} \nabla \times E)(\nabla \times \lambda)(x, t) dt + \gamma_2(\mu - \mu_0)(x).
\end{aligned} \tag{21}$$

5 Finite element method

5.1 Finite element spaces

For computations we discretize $\Omega_{\text{FEM}} \times (0, T)$ in space and time. For discretization in space we denote by $K_h = \{K\}$ a partition of the domain Ω_{FEM} into tetrahedra K in \mathbb{R}^3 or triangles in \mathbb{R}^2 . We discretize the time interval $(0, T)$ into subintervals $J = (t_{k-1}, t_k]$ of uniform length $\tau = t_k - t_{k-1}$ and denote the time partition by $J_\tau = \{J\}$. In our finite element space mesh K_h the elements K are such that

$$K_h = \cup_{K \in K_h} K = K_1 \cup K_2 \dots \cup K_l,$$

where l is the total number of elements K in $\overline{\Omega}$.

Similarly with [25] we introduce the mesh function $h = h(x)$ which is a piecewise-constant function such that

$$h|_K = h_K \quad \forall K \in K_h, \quad (22)$$

where h_K is the diameter of K which we define as the longest side of K . Let r' be the radius of the maximal circle/sphere contained in the element K . For every element $K \in K_h$ we assume the following shape regularity assumption

$$a_1 \leq h_K \leq r' a_2; \quad a_1, a_2 = \text{const.} > 0. \quad (23)$$

To formulate the finite element method for (13), we define the finite element spaces. First we introduce the finite element trial space W_h^E for every component of the electric field E defined by

$$W_h^E := \{w \in H_E^1 : w|_{K \times J} \in P_1(K) \times P_1(J), \forall K \in K_h, \forall J \in J_\tau\},$$

where $P_1(K)$ and $P_1(J)$ denote the set of linear functions on K and J , respectively. We also introduce the finite element test space W_h^λ defined by

$$W_h^\lambda := \{w \in H_\lambda^1 : w|_{K \times J} \in P_1(K) \times P_1(J), \forall K \in K_h, \forall J \in J_\tau\}.$$

To approximate the functions $\mu(x)$ and $\varepsilon(x)$ we will use the space of piecewise constant functions $V_h \subset L_2(\Omega)$,

$$V_h := \{u \in L_2(\Omega) : u|_K \in P_0(K), \forall K \in K_h\},$$

where $P_0(K)$ is the space of piecewise constant functions on K . In some numerical experiments we will use also the space of piecewise linear functions $W_h \subset H^1(\Omega)$,

$$W_h = \{v(x) \in H^1(\Omega) : v|_K \in P_1(K) \forall K \in K_h\}. \quad (24)$$

In a general case we allow the functions $\varepsilon(x), \mu(x)$ to be discontinuous, see [?]. Let F_h be the set of all faces of elements in K_h such that $F_h := F_h^I \cup F_h^B$, where F_h^I is the set of all interior faces and F_h^B is the set of all boundary faces of elements in K_h . Let $f \in F_h^I$ be the internal face of the non-empty intersection of the boundaries of two neighboring elements K^+ and K^- . We denote the jump of the function v_h computed from the two neighboring elements K^+ and K^- sharing the common side f as

$$[v_h] = v_h^+ - v_h^-, \quad (25)$$

and the jump of the normal component v_h across the side f as

$$[[v_h]] = v_h^+ \cdot n^+ + v_h^- \cdot n^-, \quad (26)$$

where n^+, n^- is the unit outward normal on f^+, f^- , respectively.

Let P_h be the $L_2(\Omega)$ orthogonal projection. We define by f_h^I the standard nodal interpolant [25] of f into the space of continuous piecewise-linear functions on the mesh K_h . Then by one of properties of the orthogonal projection

$$\|f - P_h f\|_{L_2(\Omega)} \leq \|f - f_h^I\|_{L_2(\Omega)}. \quad (27)$$

It follows from [35] that

$$\|f - P_h f\|_{L_2(\Omega)} \leq C_I h \|f\|_{H^1(\Omega)} \quad \forall f \in H^1(\Omega). \quad (28)$$

where $C_I = C_I(\Omega)$ is a positive constant depending only on the domain Ω .

5.2 A finite element method for optimization problem

To formulate the finite element method for (13) we define the space $U_h = W_h^E \times W_h^\lambda \times V_h \times V_h$. The finite element method reads: Find $u_h \in U_h$ such that

$$L'(u_h)(\bar{u}) = 0 \quad \forall \bar{u} \in U_h. \quad (29)$$

To be more precise, the equation (29) expresses that the finite element method for the forward problem (6) in Ω_{FEM} for continuous (ε, μ) will be: find $E_h = (E_{1h}, E_{2h}, E_{3h}) \in W_h^E$, such that for all $\bar{\lambda} \in W_h^\lambda$ and for the known $(\varepsilon_h, \mu_h) \in V_h \times V_h$

$$\begin{aligned} & - \left((\varepsilon_h \frac{\partial \bar{\lambda}}{\partial t} \frac{\partial E_h}{\partial t}) \right) - (\varepsilon_h f_1, \bar{\lambda}(x, 0))_\Omega + ((\mu_h^{-1} \nabla \times E_h, \nabla \times \bar{\lambda}))_{\Omega_T} + s((\nabla \cdot (\varepsilon_h E_h), \nabla \cdot \bar{\lambda}))_{\Omega_T} \\ & - ((\bar{\lambda}, p(t)))_{S_{1,1}} + ((\bar{\lambda}, \partial_t E_h))_{S_{1,2}} + ((\bar{\lambda}, \partial_t E_h))_{S_2} = 0 \quad \forall \bar{\lambda} \in H_\lambda^1(\Omega_T), \end{aligned} \quad (30)$$

and the finite element method for the adjoint problem (18) in Ω_{FEM} for continuous (ε, μ) reads: find $\lambda_h = (\lambda_{h1}, \lambda_{h2}, \lambda_{h3}) \in W_h^\lambda$, such that for the computed

approximation $E_h = (E_{1h}, E_{2h}, E_{3h}) \in W_h^E$ of (30) and for all $\bar{E} \in W_h^E$ and for the known $(\varepsilon_h, \mu_h) \in V_h \times V_h$

$$\begin{aligned} & (((E_h - \bar{E})|_{S_T} z_\delta, \bar{E})) - ((\varepsilon_h \partial_t \lambda_h, \partial_t \bar{E}))_{\Omega_T} + ((\mu_h^{-1} \nabla \times \lambda_h, \nabla \times \bar{E}))_{\Omega_T} \\ & + s((\nabla \cdot \lambda_h, \nabla \cdot (\varepsilon_h \bar{E}))_{\Omega_T} - ((\partial_t \lambda_h, \bar{E}))_{S_{1,2} \cup S_2} - (\varepsilon_h \bar{E}(x, 0), \partial_t \lambda_h(x, 0))) = 0 \quad \forall \bar{E} \in H_E^1(\Omega_T). \end{aligned} \quad (31)$$

Similar finite element method for the forward and adjoint problems can be written for discontinuous functions ε, μ which will include additional terms with jumps for computation of coefficients. In our work similarly with [17] we compute the discontinuities of coefficients ε and μ by computing the jumps from the two neighboring elements, see (25) and (26) for definitions of jumps.

Since we are usually working in finite dimensional spaces U_h and $U_h \subset U^1$ as a set, then U_h is a discrete analogue of the space U^1 . It is well known that in finite dimensional spaces all norms are equivalent, and in our computations we compute approximations of smooth functions $\varepsilon(x), \mu(x)$ in the space V_h .

5.3 Fully discrete scheme

To write fully discrete schemes for (30) and (31) we expand E_h and λ_h in terms of the standard continuous piecewise linear functions $\{\varphi_i(x)\}_{i=1}^M$ in space and $\{\psi_k(t)\}_{k=1}^N$ in time, respectively, as

$$\begin{aligned} E_h(x, t) &= \sum_{k=1}^N \sum_{i=1}^M \mathbf{E}_h \varphi_i(x) \psi_k(t), \\ \lambda_h(x, t) &= \sum_{k=1}^N \sum_{i=1}^M \lambda_h \varphi_i(x) \psi_k(t), \end{aligned}$$

where $\mathbf{E}_h := E_{h_{i,k}}$ and $\lambda_h := \lambda_{h_{i,k}}$ denote unknown coefficients at the point $x_i \in K_h$ and time level $t_k \in J_\tau$, substitute them into (30) and (31) to obtain the following system of linear equations:

$$\begin{aligned} M(\mathbf{E}^{k+1} - 2\mathbf{E}^k + \mathbf{E}^{k-1}) &= -\tau^2 K \mathbf{E}^k - s\tau^2 C \mathbf{E}^k + \tau^2 F^k + \tau^2 P^k - \frac{1}{2}\tau(MD) \cdot (\mathbf{E}^{k+1} - \mathbf{E}^{k-1}), \\ M(\boldsymbol{\lambda}^{k+1} - 2\boldsymbol{\lambda}^k + \boldsymbol{\lambda}^{k-1}) &= -\tau^2 S^k - \tau^2 K \boldsymbol{\lambda}^k - s\tau^2 C \boldsymbol{\lambda}^k + \frac{1}{2}\tau(MD) \cdot (\boldsymbol{\lambda}^{k+1} - \boldsymbol{\lambda}^{k-1}) + \tau^2 (D\boldsymbol{\lambda})^k. \end{aligned} \quad (32)$$

Here, M is the block mass matrix in space and MD is the block mass matrix in space corresponding to the elements at the boundaries $\partial_1\Omega, \partial_2\Omega$, K is the block stiffness matrix corresponding to the rotation term, C is the stiffness matrix corresponding to the divergence term, $F^k, P^k, D\boldsymbol{\lambda}^k, S^k$ are load vectors at time level

t_k , \mathbf{E}^k and $\boldsymbol{\lambda}^k$ denote the nodal values of \mathbf{E}_h and λ_h , respectively, at time level t_k , and τ is the time step. We refer to [4] for details of derivation of these matrices.

Let us define the mapping F_K for the reference element \hat{K} such that $F_K(\hat{K}) = K$ and let $\hat{\varphi}$ be the piecewise linear local basis function on the reference element \hat{K} such that $\varphi \circ F_K = \hat{\varphi}$. Then the explicit formulas for the entries in system (32) at each element K can be given as:

$$\begin{aligned}
M_{i,j}^K &= (\varepsilon_h \varphi_i \circ F_K, \varphi_j \circ F_K)_K, \\
K_{i,j}^K &= (\mu_h^{-1} \nabla \times \varphi_i \circ F_K, \nabla \times \varphi_j \circ F_K)_K, \\
C_{i,j}^K &= (\nabla \cdot (\varepsilon_h \varphi_i) \circ F_K, \nabla \cdot \varphi_j \circ F_K)_K, \\
S_j^K &= ((E_h - \tilde{E})_{S_T} z_\sigma, \varphi_j \circ F_K)_K, \\
F_j^K &= (\varepsilon_h f_1, \varphi_j \circ F_K)_K, \\
P_j^K &= (p, \varphi_j \circ F_K)_{\partial_1 \Omega_K}, \\
MD_j^K &= (\varphi_i \circ F_K, \varphi_j \circ F_K)_{\partial_1 \Omega_K \cup \partial_2 \Omega_K}, \\
D\lambda_j^K &= (\varepsilon_h \partial_t \lambda_h(x, 0), \varphi_j \circ F_K)_K,
\end{aligned}$$

where $(\cdot, \cdot)_K$ denotes the $L_2(K)$ scalar product, and $\partial_1 \Omega_K, \partial_2 \Omega_K$ are boundaries ∂K of elements K , which belong to $\partial_1 \Omega, \partial_2 \Omega$, respectively.

To obtain an explicit scheme, we approximate M with the lumped mass matrix M^L (for further details, see [19]). Next, we multiply (32) with $(M^L)^{-1}$ and get the following explicit method:

$$\begin{aligned}
(I + \frac{1}{2}\tau(M^L)^{-1}MD)\mathbf{E}^{k+1} &= 2\mathbf{E}^k - \tau^2(M^L)^{-1}K\mathbf{E}^k + \tau^2(M^L)^{-1}F^k + \tau^2(M^L)^{-1}P^k \\
&\quad + \frac{1}{2}\tau(M^L)^{-1}(MD)\mathbf{E}^{k-1} - s\tau^2(M^L)^{-1}C\mathbf{E}^k - \mathbf{E}^{k-1}, \\
(I + \frac{1}{2}\tau(M^L)^{-1}MD)\boldsymbol{\lambda}^{k+1} &= -\tau^2(M^L)^{-1}S^k + 2\boldsymbol{\lambda}^k - \tau^2(M^L)^{-1}K\boldsymbol{\lambda}^k - s\tau^2(M^L)^{-1}C\boldsymbol{\lambda}^k \\
&\quad + \tau^2(M^L)^{-1}(D\boldsymbol{\lambda})^k - \boldsymbol{\lambda}^{k+1} + \frac{1}{2}\tau(M^L)^{-1}(MD)\boldsymbol{\lambda}^{k+1}.
\end{aligned} \tag{33}$$

In the case of the domain decomposition FEM/FDM method when the schemes above are used only in Ω_{FEM} we have

$$\begin{aligned}
\mathbf{E}^{k+1} &= 2\mathbf{E}^k - \tau^2(M^L)^{-1}K\mathbf{E}^k + \tau^2(M^L)^{-1}F^k + \tau^2(M^L)^{-1}P^k - s\tau^2(M^L)^{-1}C\mathbf{E}^k - \mathbf{E}^{k-1}, \\
\boldsymbol{\lambda}^{k+1} &= -\tau^2(M^L)^{-1}S^k + 2\boldsymbol{\lambda}^k - \tau^2(M^L)^{-1}K\boldsymbol{\lambda}^k - s\tau^2(M^L)^{-1}C\boldsymbol{\lambda}^k + \tau^2(M^L)^{-1}D\boldsymbol{\lambda} - \boldsymbol{\lambda}^{k+1}.
\end{aligned} \tag{34}$$

6 Relaxation property of mesh refinements

In this section we reformulate results of [10] for the case of our **IP**. For simplicity, we shall sometimes write $\|\cdot\|$ for the L_2 norm.

We use the theory of ill-posed problems [38, 39] and introduce noise level δ in the function $\tilde{E}(x, t)$ in the Tikhonov functional (9). This means that

$$\tilde{E}(x, t) = \tilde{E}^*(x, t) + \tilde{E}_\delta(x, t); \quad \tilde{E}^*, \tilde{E}_\delta \in L_2(S_T) = H_2, \quad (35)$$

where $\tilde{E}^*(x, t)$ is the exact data corresponding to the exact function $z^* = (\varepsilon^*, \mu^*)$, and the function $\tilde{E}_\delta(x, t)$ represents the error in these data. In other words, we can write that

$$\left\| \tilde{E}_\delta \right\|_{L_2(S_T)} \leq \delta. \quad (36)$$

The question of stability and uniqueness of our **IP** is addressed in [6, 12] which is needed in the local strong convexity theorem formulated below. Let H_1 be the finite dimensional linear space. Let Y be the set of admissible functions (ε, μ) which we defined in (7), and let $Y_1 := Y \cap H_1$ with $G := \bar{Y}_1$. We introduce now the operator $F : G \rightarrow H_2$ corresponding to the Tikhonov functional (9) such that

$$F(z)(x, t) := F(\varepsilon, \mu)(x, t) = (E(x, t, \varepsilon, \mu) - \tilde{E})^2 z_\delta(t) \quad \forall (x, t) \in S_T, \quad (37)$$

where $E(x, t, \varepsilon, \mu) := E(x, t)$ is the weak solution of the forward problem (6) and thus, depends on ε and μ . Here, $z = (\varepsilon, \mu)$ and $z_\delta(t)$ is a cut-off function chosen as in [6].

We now assume that the operator $F(z)(x, t)$ which we defined in (37) is one-to-one. Let us denote by

$$V_d(z) = \{z' \in H_1 : \|z' - z\| < d \quad \forall z = (\varepsilon, \mu) \in H_1\} \quad (38)$$

the neighborhood of z of the diameter d . We also assume that the operator F is Lipschitz continuous what means that for $N_1, N_2 > 0$

$$\|F'(z)\| \leq N_1, \quad \|F'(z_1) - F'(z_2)\| \leq N_2 \|z_1 - z_2\| \quad \forall z_1, z_2 \in V_1(z^*). \quad (39)$$

Let the constant $D = D(N_1, N_2) = \text{const.} > 0$ is such that

$$\|J'(z_1) - J'(z_2)\| \leq D \|z_1 - z_2\| \quad \forall z_1, z_2 \in V_1(z^*), \quad (40)$$

where (ε^*, μ^*) is the exact solution of the equation $F(\varepsilon^*, \mu^*) = 0$. Similarly with [10], we assume that

$$\begin{aligned} \|\varepsilon_0 - \varepsilon^*\| &\leq \delta^{\nu_1}, \quad \nu_1 = \text{const.} \in (0, 1), \\ \|\mu_0 - \mu^*\| &\leq \delta^{\nu_2}, \quad \nu_2 = \text{const.} \in (0, 1), \\ \gamma_1 &= \delta^{\zeta_1}, \quad \zeta_1 = \text{const.} \in (0, \min(\nu_1, 2(1 - \nu_1))), \\ \gamma_2 &= \delta^{\zeta_2}, \quad \zeta_2 = \text{const.} \in (0, \min(\nu_2, 2(1 - \nu_2))), \end{aligned} \quad (41)$$

which in closed form can be written as

$$\begin{aligned} \|z_0 - z^*\| &\leq \delta^{(\nu_1, \nu_2)}, \quad z_0 = (\varepsilon_0, \mu_0), \quad (\nu_1, \nu_2) = \text{const.} \in (0, 1), \\ (\gamma_1, \gamma_2) &= \delta^{(\zeta_1, \zeta_2)}, \quad (\zeta_1, \zeta_2) = \text{const.} \in (0, \min((\nu_1, \nu_2), 2(1 - (\nu_1, \nu_2)))) \end{aligned} \quad (42)$$

where (γ_1, γ_2) are regularization parameters in (9). Equation (42) means that we assume that all initial guesses $z_0 = (\varepsilon_0, \mu_0)$ are located in a sufficiently small neighborhood $V_{\delta^{\mu_1}}(z^*)$ of the exact solution $z^* = (\varepsilon^*, \mu^*)$. Conditions (43) imply that (z^*, z_0) belong to an appropriate neighborhood of the regularized solution of the functional (9), see proofs in Lemmata 2.1 and 3.2 of [10].

Below we reformulate Theorem 1.9.1.2 of [9] for the Tikhonov functional (9). Different proofs of it can be found in [9] and in [10] and are straightly applied to our **IP**. We note here that if functions $(\varepsilon, \mu) \in H_1$ and satisfy conditions (7) then $(\varepsilon, \mu) \in \text{Int}(G)$.

Theorem 1 *Let $\Omega \subset \mathbb{R}^3$ be a convex bounded domain with the boundary $\partial\Omega \in C^3$. Suppose that conditions (35) and (36) hold. Let the function $E(x, t) \in H^2(\Omega_T)$ in the Tikhonov functional (9) be the solution of the forward problem (6) for the functions $(\varepsilon, \mu) \in G$. Assume that there exists the exact solutions $(\varepsilon^*, \mu^*) \in G$ of the equation $F(\varepsilon^*, \mu^*) = 0$ for the case of the exact data \tilde{E}^* in (35). Let regularization parameters (γ_1, γ_2) in (9) are such that*

$$(\gamma_1, \gamma_2) = (\gamma_1, \gamma_2)(\delta) = \delta^{2(\nu_1, \nu_2)}, \quad (\nu_1, \nu_2) = \text{const.} \in \left(0, \frac{1}{4}\right) \quad \forall \delta \in (0, 1).$$

Let $z_0 = (\varepsilon_0, \mu_0)$ satisfy (42). Then the Tikhonov functional (9) is strongly convex in the neighborhood $V_{(\gamma_1, \gamma_2)(\delta)}(\varepsilon^, \mu^*)$ with the strong convexity constants $(\alpha_1, \alpha_2) = (\gamma_1, \gamma_2)/2$. The strong convexity property can be also written as*

$$\|z_1 - z_2\|^2 \leq \frac{2}{\delta^{2(\nu_1, \nu_2)}} (J'(z_1) - J'(z_2), z_1 - z_2) \quad \forall z_1 = (\varepsilon_1, \mu_1), z_2 = (\varepsilon_2, \mu_2) \in H_1. \quad (44)$$

Alternatively, using the expression for the Fréchet derivative given in (20) we can write (44) as

$$\begin{aligned} \|\varepsilon_1 - \varepsilon_2\|^2 &\leq \frac{2}{\delta^{2\nu_1}} (J'_\varepsilon(\varepsilon_1, \mu_1) - J'_\varepsilon(\varepsilon_2, \mu_2), \varepsilon_1 - \varepsilon_2) \quad \forall (\varepsilon_1, \mu_1), (\varepsilon_2, \mu_2) \in H_1, \\ \|\mu_1 - \mu_2\|^2 &\leq \frac{2}{\delta^{2\nu_2}} (J'_\mu(\varepsilon_1, \mu_1) - J'_\mu(\varepsilon_2, \mu_2), \mu_1 - \mu_2) \quad \forall (\varepsilon_1, \mu_1), (\varepsilon_2, \mu_2) \in H_1, \end{aligned} \quad (45)$$

where (\cdot, \cdot) is the $L_2(\Omega)$ inner product. Next, there exists the unique regularized solution $(\varepsilon_{\gamma_1}, \mu_{\gamma_2})$ of the functional (9) in $(\varepsilon_{\gamma_1}, \mu_{\gamma_2}) \in V_{\delta^{3(\nu_1, \nu_2)}/3}(\varepsilon^, \mu^*)$. The gradient method of the minimization of the functional (9) which starts at (ε_0, μ_0) converges to the regularized solution of this functional. Furthermore,*

$$\begin{aligned}\|\varepsilon_{\gamma_1} - \varepsilon^*\| &\leq \Theta_1 \|\varepsilon_0 - \varepsilon^*\|, \quad \Theta_1 \in (0, 1), \\ \|\mu_{\gamma_2} - \mu^*\| &\leq \Theta_2 \|\mu_0 - \mu^*\|, \quad \Theta_2 \in (0, 1).\end{aligned}\tag{46}$$

The property(46) means that the regularized solution of the Tikhonov functional (9) provides a better accuracy than the initial guess (ε_0, μ_0) if it satisfies condition (42). The next theorem presents the estimate of the norm $\|(\varepsilon, \mu) - (\varepsilon_{\gamma_1}, \mu_{\gamma_2})\|$ via the norm of the Fréchet derivative of the Tikhonov functional (9).

Theorem 2 *Assume that conditions of Theorem 1 hold. Then for any functions $(\varepsilon, \mu) \in V_{(\gamma_1, \gamma_2)(\delta)}(\varepsilon^*, \mu^*)$ the following error estimate holds*

$$\|(\varepsilon, \mu) - (\varepsilon_{\gamma_1(\delta)}, \mu_{\gamma_2(\delta)})\| \leq \frac{2}{\delta^{2(\nu_1, \nu_2)}} \|P_h J'(\varepsilon, \mu)\| \leq \frac{2}{\delta^{2(\nu_1, \nu_2)}} \|J'(\varepsilon, \mu)\|, \tag{47}$$

which explicitly can be written as

$$\begin{aligned}\|\varepsilon - \varepsilon_{\gamma_1(\delta)}\| &\leq \frac{2}{\delta^{2\nu_1}} \|P_h J'_\varepsilon(\varepsilon, \mu)\| \leq \frac{2}{\delta^{2\nu_1}} \|J'_\varepsilon(\varepsilon, \mu)\| = \frac{2}{\delta^{2\nu_1}} \|L'_\varepsilon(u(\varepsilon, \mu))\|, \\ \|\mu - \mu_{\gamma_2(\delta)}\| &\leq \frac{2}{\delta^{2\nu_2}} \|P_h J'_\mu(\varepsilon, \mu)\| \leq \frac{2}{\delta^{2\nu_2}} \|J'_\mu(\varepsilon, \mu)\| = \frac{2}{\delta^{2\nu_2}} \|L'_\mu(u(\varepsilon, \mu))\|,\end{aligned}\tag{48}$$

where $(\varepsilon_{\gamma_1(\delta)}, \mu_{\gamma_2(\delta)})$ are minimizers of the Tikhonov functional (9) computed with regularization parameters $(\gamma_1(\delta), \gamma_2(\delta))$ and $P_h : L_2(\Omega) \rightarrow H_1$ is the operator of orthogonal projection of the space $L_2(\Omega)$ on its subspace H_1 .

Proof.

Since $(\varepsilon_{\gamma_1}, \mu_{\gamma_2}) := (\varepsilon_{\gamma_1(\delta)}, \mu_{\gamma_2(\delta)})$ is the minimizer of the functional (9) on the set G and $(\varepsilon_{\gamma_1}, \mu_{\gamma_2}) \in \text{Int}(G)$, then $P_h J'(\varepsilon_{\gamma_1}, \mu_{\gamma_2}) = 0$, or

$$\begin{aligned}P_h J'_\varepsilon(\varepsilon_{\gamma_1}, \mu_{\gamma_2}) &= 0, \\ P_h J'_\mu(\varepsilon_{\gamma_1}, \mu_{\gamma_2}) &= 0.\end{aligned}\tag{49}$$

Similarly with Theorem 4.11.2 of [9] since $(\varepsilon, \mu) - (\varepsilon_{\gamma_1}, \mu_{\gamma_2}) \in H_1$, then

$$(J'(\varepsilon, \mu) - J'(\varepsilon_{\gamma_1}, \mu_{\gamma_2}), (\varepsilon, \mu) - (\varepsilon_{\gamma_1}, \mu_{\gamma_2})) = (P_h J'(\varepsilon, \mu) - P_h J'(\varepsilon_{\gamma_1}, \mu_{\gamma_2}), (\varepsilon, \mu) - (\varepsilon_{\gamma_1}, \mu_{\gamma_2})).$$

Hence, using (44) and (49) we can write that

$$\begin{aligned}\|(\varepsilon, \mu) - (\varepsilon_{\gamma_1}, \mu_{\gamma_2})\|^2 &\leq \frac{2}{\delta^{2(\nu_1, \nu_2)}} (J'(\varepsilon, \mu) - J'(\varepsilon_{\gamma_1}, \mu_{\gamma_2}), (\varepsilon, \mu) - (\varepsilon_{\gamma_1}, \mu_{\gamma_2})) \\ &= \frac{2}{\delta^{2(\nu_1, \nu_2)}} (P_h J'(\varepsilon, \mu) - P_h J'(\varepsilon_{\gamma_1}, \mu_{\gamma_2}), (\varepsilon, \mu) - (\varepsilon_{\gamma_1}, \mu_{\gamma_2})) \\ &= \frac{2}{\delta^{2(\nu_1, \nu_2)}} (P_h J'(\varepsilon, \mu), (\varepsilon, \mu) - (\varepsilon_{\gamma_1}, \mu_{\gamma_2})) \\ &\leq \frac{2}{\delta^{2(\nu_1, \nu_2)}} \|P_h J'(\varepsilon, \mu)\| \cdot \|(\varepsilon, \mu) - (\varepsilon_{\gamma_1}, \mu_{\gamma_2})\|.\end{aligned}$$

Thus, from the expression above we can get

$$\|(\varepsilon, \mu) - (\varepsilon_{\gamma_1}, \mu_{\gamma_2})\|^2 \leq \frac{2}{\delta^{2(\nu_1, \nu_2)}} \|P_h J'(\varepsilon, \mu)\| \cdot \|(\varepsilon, \mu) - (\varepsilon_{\gamma_1}, \mu_{\gamma_2})\|.$$

We now divide the expression above by $\|(\varepsilon, \mu) - (\varepsilon_{\gamma_1}, \mu_{\gamma_2})\|$. Using the fact that

$$\|P_h J'(\varepsilon, \mu)\| \leq \|J'(\varepsilon, \mu)\|,$$

we obtain (47), and using definition of the derivative of the Tikhonov functional (20) we get (48), where explicit entries of $L'_\varepsilon(u(\varepsilon, \mu))$, $L'_\mu(u(\varepsilon, \mu))$ are given by (16), (17), respectively.

□

Below we reformulate Lemmas 2.1 and 3.2 of [10] for the case of Tikhonov functional (9).

Theorem 3 *Let the assumptions of Theorems 1,2 hold. Let $\|(\varepsilon^*, \mu^*)\| \leq C$, with a given constant C . We define by $M_n \subset H_1$ the subspace which is obtained after n mesh refinements of the mesh K_h . Let h_n be the mesh function on M_n as defined in Section 5. Then there exists the unique minimizer $(\varepsilon_n, \mu_n) \in G \cap M_n$ of the Tikhonov functional (9) such that the following inequalities hold*

$$\begin{aligned} \|\varepsilon_n - \varepsilon_{\gamma_1(\delta)}\| &\leq \frac{2}{\delta^{2\nu_1}} \|J'_\varepsilon(\varepsilon, \mu)\|, \\ \|\mu_n - \mu_{\gamma_2(\delta)}\| &\leq \frac{2}{\delta^{2\nu_2}} \|J'_\mu(\varepsilon, \mu)\|. \end{aligned} \tag{50}$$

Now we present relaxation property of mesh refinements for the Tikhonov functional (9) which follows from the Theorem 4.1 of [10].

Theorem 4 . *Let the assumptions of Theorems 2, 3 hold. Let $(\varepsilon_n, \mu_n) \in V_{\delta^{3\mu}}(\varepsilon^*, \mu^*) \cap M_n$ be the minimizer of the Tikhonov functional (9) on the set $G \cap M_n$. The existence of the minimizer is guaranteed by Theorem 3. Assume that the regularized solution $(\varepsilon, \mu) \neq (\varepsilon_n, \mu_n)$ which means that $(\varepsilon, \mu) \notin M_n$. Then the following relaxation properties hold*

$$\begin{aligned} \|\varepsilon_{n+1} - \varepsilon\| &\leq \eta_{1,n} \|\varepsilon_n - \varepsilon\|, \\ \|\mu_{n+1} - \mu\| &\leq \eta_{2,n} \|\mu_n - \mu\| \end{aligned}$$

for $\eta_{1,n}, \eta_{2,n} \in (0, 1)$.

7 General framework of a posteriori error estimate

In this section we briefly present a posteriori error estimates for three kinds of errors:

- for the error $|L(u) - L(u_h)|$ in the Lagrangian (11);
- for the error $|J(\varepsilon, \mu) - J(\varepsilon_h, \mu_h)|$ in the Tikhonov functional (9);
- for the errors $|\varepsilon - \varepsilon_h|$ and $|\mu - \mu_h|$ in the regularized solutions ε, μ of this functional.

Here, $u_h, \varepsilon_h, \mu_h$ are finite element approximations of the functions u, ε, μ , respectively. A posteriori error estimate in the Lagrangian was already derived in [5] for the case when only the function $\varepsilon(x)$ in system (6) is unknown. In [13, 14] were derived a posteriori error estimates in the Lagrangian which corresponds to modified system (6) for $\mu = 1$. A posteriori error in the Lagrangian (11) can be derived straightforwardly from a posteriori error estimate presented in [5] and thus, all details of this derivation are not presented here.

However, to make clear how a posteriori errors in the Lagrangian and in the Tikhonov functional can be obtained, we present general framework for them. First we note that

$$\begin{aligned} J(\varepsilon, \mu) - J(\varepsilon_h, \mu_h) &= J'_\varepsilon(\varepsilon_h, \mu_h)(\varepsilon - \varepsilon_h) + J'_\mu(\varepsilon_h, \mu_h)(\mu - \mu_h) + R(\varepsilon, \varepsilon_h) + R(\mu, \mu_h), \\ L(u) - L(u_h) &= L'(u_h)(u - u_h) + R(u, u_h), \end{aligned} \tag{51}$$

where $R(\varepsilon, \varepsilon_h), R(\mu, \mu_h), R(u, u_h)$, are remainders of the second order. We assume that (ε_h, μ_h) are located in the small neighborhood of the regularized solutions (ε, μ) , correspondingly. Thus, since the terms $R(u, u_h), R(\varepsilon, \varepsilon_h), R(\mu, \mu_h)$ are of the second order then they will be small and we can neglect them in (51).

We now use the splitting

$$\begin{aligned} u - u_h &= (u - u_h^I) + (u_h^I - u_h), \\ \varepsilon - \varepsilon_h &= (\varepsilon - \varepsilon_h^I) + (\varepsilon_h^I - \varepsilon_h), \\ \mu - \mu_h &= (\mu - \mu_h^I) + (\mu_h^I - \mu_h), \end{aligned} \tag{52}$$

together with the Galerkin orthogonality principle

$$\begin{aligned} L'(u_h)(\bar{u}) &= 0 \quad \forall \bar{u} \in U_h, \\ J'(z_h)(b) &= 0 \quad \forall b \in V_h, \end{aligned} \tag{53}$$

insert (52) into (51) and get the following error representations:

$$\begin{aligned} L(u) - L(u_h) &\approx L'(u_h)(u - u_h^I), \\ J(\varepsilon, \mu) - J(\varepsilon_h, \mu_h) &\approx J'_\varepsilon(\varepsilon_h, \mu_h)(\varepsilon - \varepsilon_h^I) + J'_\mu(\varepsilon_h, \mu_h)(\mu - \mu_h^I). \end{aligned} \tag{54}$$

In (52), (54) functions $u_h^I \in U_h$ and $\varepsilon_h^I, \mu_h^I \in V_h$ denote the interpolants of u, ε, μ , respectively.

Using (54) we conclude that a posteriori error estimate in the Lagrangian involves the derivative of the Lagrangian $L'(u_h)$ which we define as a residual, multiplied by weights $u - u_h^I$. Similarly, a posteriori error estimate in the Tikhonov functional involves the derivatives of the Tikhonov functional $J'_\varepsilon(\varepsilon_h, \mu_h)$ and $J'_\mu(\varepsilon_h, \mu_h)$ which represents residuals, multiplied by weights $\varepsilon - \varepsilon_h^I$ and $\mu - \mu_h^I$, correspondingly.

To derive the errors $|\varepsilon - \varepsilon_h|$ and $|\mu - \mu_h|$ in the regularized solutions ε, μ of the functional (9) we will use the convexity property of the Tikhonov functional together with the interpolation property (28). We now make both error estimates more explicit.

8 A posteriori error estimate in the regularized solution

In this section we formulate theorem for a posteriori error estimates $|\varepsilon - \varepsilon_h|$ and $|\mu - \mu_h|$ in the regularized solution ε, μ of the functional (9). During the proof we reduce notations and denote the scalar product $(\cdot, \cdot)_{L_2}$ as (\cdot, \cdot) , as well as we denote the norm $\|\cdot, \cdot\|_{L_2}$ as $\|\cdot, \cdot\|$. However, if norm should be specified, we will write it explicitly.

Theorem 5

Let the assumptions of Theorems 1,2 hold. Let $z_h = (\varepsilon_h, \mu_h) \in W_h$ be a finite element approximations of the regularized solution $z = (\varepsilon, \mu)$ on the finite element mesh K_h . Then there exists a constant D defined in (40) such that the following a posteriori error estimates hold

$$\begin{aligned} \|\varepsilon - \varepsilon_h\| &\leq \frac{D}{\alpha_1} C_I (h \|\varepsilon_h\| + \|[\varepsilon_h]\|) = \frac{2D}{\delta^{2\nu_1}} C_I (h \|\varepsilon_h\| + \|[\varepsilon_h]\|) \quad \forall \varepsilon_h \in V_h, \\ \|\mu - \mu_h\| &\leq \frac{D}{\alpha_2} C_I (h \|\mu_h\| + \|[\mu_h]\|) = \frac{2D}{\delta^{2\nu_2}} C_I (h \|\mu_h\| + \|[\mu_h]\|) \quad \forall \mu_h \in V_h. \end{aligned} \tag{55}$$

Proof.

Let $z_h = (\varepsilon_h, \mu_h)$ be the minimizer of the Tikhonov functional (9). The existence and uniqueness of this minimizer is guaranteed by Theorem 2. By the Theorem 1, the functional (9) is strongly convex on the space L_2 with the strong convexity constants $(\alpha_1, \alpha_2) = (\gamma_1/2, \gamma_2/2)$. This fact implies, see (44), that

$$(\alpha_1, \alpha_2) \|z - z_h\|_{L_2(\Omega)}^2 \leq (J'(z) - J'(z_h), z - z_h), \tag{56}$$

where $J'(z_h), J'(z)$ are the Fréchet derivatives of the functional (9).

Using (56) with the splitting

$$z - z_h = (z - z_h^I) + (z_h^I - z_h),$$

where z_h^I is the standard interpolant of z , and combining it with the Galerkin orthogonality principle

$$(J'(z_h) - J'(z), z_h^I - z_h) = 0 \quad (57)$$

such that $(z_h, z_h^I) \in W_h$, we will obtain

$$(\alpha_1, \alpha_2) \|z - z_h\|_{L_2}^2 \leq (J'(z) - J'(z_h), z - z_h^I). \quad (58)$$

The right-hand side of (58) can be estimated using (40) as

$$(J'(z) - J'(z_h), z - z_h^I) \leq D \|z - z_h\| \cdot \|z - z_h^I\|.$$

Substituting above equation into (58) we obtain

$$\|z - z_h\| \leq \frac{D}{(\alpha_1, \alpha_2)} \|z - z_h^I\|. \quad (59)$$

Using the interpolation property (28)

$$\|z - z_h^I\|_{L^2(\Omega)} \leq C_I h \|z\|_{H^1(\Omega)}$$

we get a posteriori error estimate for the regularized solution z with the interpolation constant C_I :

$$\|z - z_h\| \leq \frac{D}{(\alpha_1, \alpha_2)} \|z - z_h^I\| \leq \frac{D}{(\alpha_1, \alpha_2)} C_I h \|z\|_{H^1(\Omega)}. \quad (60)$$

We can estimate $h \|z\|_{H^1(\Omega)}$ as

$$\begin{aligned} h \|z\|_{H^1(\Omega)} &\leq \sum_K h_K \|z\|_{H^1(K)} = \sum_K \|(z + \nabla z)\|_{L_2(K)} h_K \\ &\leq \sum_K \left(h_K \|z_h\|_{L_2(K)} + \left\| \frac{[z_h]}{h_K} h_K \right\|_{L_2(K)} \right) \\ &\leq h \|z_h\|_{L_2(\Omega)} + \sum_K (\|[z_h]\|_{L_2(K)}). \end{aligned} \quad (61)$$

We denote in (61) by $[z_h]$ the jump of the function z_h over the element K , h_K is the diameter of the element K . In (61) we also used the fact that [27]

$$|\nabla z| \leq \frac{[z_h]}{h_K}. \quad (62)$$

Substituting the above estimates into the right-hand side of (60) we get

$$\|z - z_h\| \leq \frac{D}{(\alpha_1, \alpha_2)} C_I h \|z_h\| + \frac{D}{(\alpha_1, \alpha_2)} C_I \|[z_h]\| \quad \forall z_h \in W_h.$$

Now taking into account $z_h = (\varepsilon_h, \mu_h)$ we get estimate (55) for $|\varepsilon - \varepsilon_h|$ and $|\mu - \mu_h|$, correspondingly.

□

9 A posteriori error estimates for the Tikhonov functional

In Theorem 2 we derive a posteriori error estimates for the error in the Tikhonov functional (9) obtained on the finite element mesh K_h .

Theorem 6

Suppose that there exists minimizer $(\varepsilon, \mu) \in H^1(\Omega)$ of the Tikhonov functional (9) on the mesh K_h . Suppose also that there exists a finite element approximation $z_h = (\varepsilon_h, \mu_h)$ of $z = (\varepsilon, \mu)$ of $J(\varepsilon, \mu)$ on the set W_h and mesh K_h with the mesh function h . Then the following approximate a posteriori error estimate for the error $e = |J(\varepsilon, \mu) - J(\varepsilon_h, \mu_h)|$ in the Tikhonov functional (9) holds

$$\begin{aligned} e = |J(\varepsilon, \mu) - J(\varepsilon_h, \mu_h)| &\leq C_I (\|J'_\varepsilon(\varepsilon_h, \mu_h)\| (h\|\varepsilon_h\| + \|[\varepsilon_h]\|) \\ &\quad + \|J'_\mu(\varepsilon_h, \mu_h)\| (h\|\mu_h\| + \|[\mu_h]\|)) \\ &= C_I (\|L'_\varepsilon(u(\varepsilon_h, \mu_h))\| (h\|\varepsilon_h\| + \|[\varepsilon_h]\|) \\ &\quad + \|L'_\mu(u(\varepsilon_h, \mu_h))\| (h\|\mu_h\| + \|[\mu_h]\|)). \end{aligned} \quad (63)$$

Proof

By the definition of the Fréchet derivative of the Tikhonov functional (9) with $z = (\varepsilon, \mu)$, $z_h = (\varepsilon_h, \mu_h)$ we can write that on the mesh K_h

$$J(z) - J(z_h) = J'(z_h)(z - z_h) + R(z, z_h), \quad (64)$$

where remainder $R(z, z_h) = O((z - z_h)^2)$, $(z - z_h) \rightarrow 0 \quad \forall z, z_h \in W_h$ and $J'(z_h)$ is the Fréchet derivative of the functional (9). We can neglect the term $R(z, z_h)$ in the estimate (64) since it is small. This is because we assume that z_h is the minimizer of the Tikhonov functional on the mesh K_h and this minimizer is located in a small neighborhood of the regularized solution z . For similar results for the case of a general nonlinear operator equation we refer to [2, 10]. We again use the splitting

$$z - z_h = z - z_h^I + z_h^I - z_h \quad (65)$$

and the Galerkin orthogonality [25]

$$J'(z_h)(z_h^I - z_h) = 0 \quad \forall z_h^I, z_h \in W_h \quad (66)$$

to get

$$J(z) - J(z_h) \leq J'(z_h)(z - z_h^I), \quad (67)$$

where z_h^I is a standard interpolant of z on the mesh K_h [25]. Using (67) we can also write

$$|J(z) - J(z_h)| \leq \|J'(z_h)\| \cdot \|z - z_h^I\|, \quad (68)$$

where the term $\|z - z_h^I\|$ can be estimated through the interpolation estimate

$$\|z - z_h^I\|_{L_2(\Omega)} \leq C_I \|h z\|_{H^1(\Omega)}.$$

Substituting above estimate into (68) we get

$$|J(z) - J(z_h)| \leq C_I \|J'(z_h)\| h \|z\|_{H^1(\Omega)}. \quad (69)$$

Using (62) we can estimate $h \|z\|_{H^1(\Omega)}$ similarly with (61) to get

$$|J(z) - J(z_h)| \leq C_I \|J'(z_h)\| (h \|z_h\| + \|[z_h]\|) \quad \forall z_h \in W_h. \quad (70)$$

Now taking into account $z_h = (\varepsilon_h, \mu_h)$ and using (20) we get estimate (63) for $|J(\varepsilon, \mu) - J(\varepsilon_h, \mu_h)|$.

□

10 Mesh refinement recommendations

In this section we will show how to use Theorems 5 and 6 for the local mesh refinement recommendation. This recommendation will allow improve accuracy of the reconstruction of the regularized solution (ε, μ) of our problem **IP**.

Using the estimate (55) we observe that the main contributions of the norms of the reconstructed functions (ε_h, μ_h) are given by neighborhoods of thus points in the finite element mesh K_h where computed values of $|h\varepsilon_h|$ and $|h\mu_h|$ achieve its maximal values.

We also note that terms with jumps in the estimate (55) disappear in the case of the conforming finite element meshes and with $(\varepsilon_h, \mu_h) \in V_h$. Our idea of the local finite element mesh refinement is that it should be refined all neighborhoods of all points in the mesh K_h where the functions $|h\varepsilon_h|$ and $|h\mu_h|$ achieves its maximum values.

Similarly, the estimate (63) of Theorem 6 gives us the idea where locally refine the finite element mesh K_h to improve the accuracy in the Tikhonov functional (9).

Using the estimate (63) we observe that the main contributions of the norms in the right-hand side of (63) are given by neighborhoods of thus points in the finite element mesh K_h where computed values of $|h\varepsilon_h|$, $|h\mu_h|$, as well as computed values of $|J'_\varepsilon(\varepsilon_h, \mu_h)|$, $|J'_\mu(\varepsilon_h, \mu_h)|$ achieve its maximal values.

Recalling (20) and (16), (17) we have

$$J'_\varepsilon(\varepsilon_h, \mu_h)(x) = - \int_0^T (\partial_t \lambda \partial_t E)(x, t) dt + s \int_0^T (\nabla \cdot E)(\nabla \cdot \lambda)(x, t) dt - \lambda(x, 0)f_1(x) + \gamma_1(\varepsilon_h - \varepsilon_0)(x), \quad x \in \Omega, \quad (71)$$

$$J'_\mu(\varepsilon_h, \mu_h)(x) = - \int_0^T (\mu_h^{-2} \nabla \times E \nabla \times \lambda)(x, t) dt + \gamma_2(\mu_h - \mu_0)(x), \quad x \in \Omega. \quad (72)$$

Thus, the second idea where to refine the finite element mesh K_h is that the neighborhoods of all points in K_h where $|J'_\varepsilon(\varepsilon_h, \mu_h)| + |J'_\mu(\varepsilon_h, \mu_h)|$ achieve its maximum, or both functions $|h\varepsilon_h| + |h\mu_h|$ and $|J'_\varepsilon(\varepsilon_h, \mu_h)| + |J'_\mu(\varepsilon_h, \mu_h)|$ achieve their maximum, should be refined. We include the term $|h\varepsilon_h| + |h\mu_h|$ in the first mesh refinement recommendation, and the term $|J'_\varepsilon(\varepsilon_h, \mu_h)| + |J'_\mu(\varepsilon_h, \mu_h)|$ in the second mesh refinement recommendation. In our computations of Section 12 we use the first mesh refinement recommendation and check performance of this mesh refinement criteria.

The First Mesh Refinement Recommendation for IP. *Applying Theorem 5 we conclude that we should refine the mesh in neighborhoods of those points in Ω_{FEM} where the function $|h\varepsilon_h| + |h\mu_h|$ attains its maximal values. More precisely, we refine the mesh in such subdomains of Ω_{FEM} where*

$$|h\varepsilon_h| + |h\mu_h| \geq \tilde{\beta} \max_{\Omega_{FEM}} (|h\varepsilon_h| + |h\mu_h|),$$

where $\tilde{\beta} \in (0, 1)$ is the number which should be chosen computationally and h is the mesh function (22) of the finite element mesh K_h .

The Second Mesh Refinement Recommendation for IP. *Using Theorem 6 we conclude that we should refine the mesh in neighborhoods of those points in Ω_{FEM} where the function $|J'_\varepsilon(\varepsilon_h, \mu_h)| + |J'_\mu(\varepsilon_h, \mu_h)|$ attains its maximal values. More precisely, let $\beta \in (0, 1)$ be the tolerance number which should be chosen in computational experiments. Refine the mesh K_h in such subdomains of Ω_{FEM} where*

$$|J'_\varepsilon(\varepsilon_h, \mu_h) + J'_\mu(\varepsilon_h, \mu_h)| \geq \beta \max_{\Omega_{FEM}} (|J'_\varepsilon(\varepsilon_h, \mu_h) + J'_\mu(\varepsilon_h, \mu_h)|).$$

Remarks

- 1. We note that in (71), (72) we have exact values of $E(x, t)$, $\lambda(x, t)$ obtained with the computed functions (ε_h, μ_h) . However, in our algorithms of Section 11 and in computations of Section 12 we approximate exact values of $E(x, t)$, $\lambda(x, t)$ by the computed ones $E_h(x, t)$, $\lambda_h(x, t)$.

- 2. In both mesh refinement recommendations we used the fact that functions ε, μ are unknown only in Ω_{FEM} .

11 Algorithms for solution IP

In this section we will present three different algorithms which can be used for solution of our **IP**: usual conjugate gradient algorithm and two different adaptive finite element algorithms. Conjugate gradient algorithm is applied on every finite element mesh K_h which we use in computations. We note that in our adaptive algorithms we refine not only the space mesh K_h but also the time mesh J_τ accordingly to the CFL condition of [18]. However, the time mesh J_τ is refined globally and not locally. It can be thought as a new research task to check how will adaptive finite element method work when both space and time meshes are refined locally.

Taking into account remark of Section 10 we denote by

$$g_\varepsilon^n(x) = - \int_0^T (\partial_t \lambda_h \partial_t E_h)(x, t, \varepsilon_h^n, \mu_h^n) dt + s \int_0^T (\nabla \cdot E_h)(\nabla \cdot \lambda_h)(x, t, \varepsilon_h^n, \mu_h^n) dt - \lambda_h(x, 0) f_1(x) + \gamma_1(\varepsilon_h^n - \varepsilon_0)(x), \quad x \in \Omega, \quad (73)$$

$$g_\mu^n(x) = - \int_0^T ((\mu_h^n)^{-2} \nabla \times E_h \nabla \times \lambda_h)(x, t, \varepsilon_h^n, \mu_h^n) dt + \gamma_2(\mu_h^n - \mu_0)(x), \quad x \in \Omega, \quad (74)$$

where functions λ_h, E_h are approximated finite element solutions of state and adjoint problems computed with $\varepsilon := \varepsilon_h^n$ and $\mu := \mu_h^n$, respectively, and n is the number of iteration in the conjugate gradient algorithm.

11.1 Conjugate Gradient Algorithm

- Step 0. Discretize the computational space-time domain $\Omega \times [0, T]$ using partitions K_h and J_τ , respectively, see Section 5. Start with the initial approximations $\varepsilon_h^0 = \varepsilon_0$ and $\mu_h^0 = \mu_0$ and compute the sequences of ε_h^n, μ_h^n as:
- Step 1. Compute solutions $E_h(x, t, \varepsilon_h^n, \mu_h^n)$ and $\lambda_h(x, t, \varepsilon_h^n, \mu_h^n)$ of state (6) and adjoint (18) problems, respectively, using explicit schemes (34).
- Step 2. Update the coefficient $\varepsilon_h := \varepsilon_h^{n+1}$ and $\mu_h := \mu_h^{n+1}$ on K_h and J_τ via the conjugate gradient method

$$\begin{aligned} \varepsilon_h^{n+1} &= \varepsilon_h^n + \alpha_\varepsilon d_\varepsilon^n(x), \\ \mu_h^{n+1} &= \mu_h^n + \alpha_\mu d_\mu^n(x), \end{aligned}$$

where

$$\begin{aligned} d_\varepsilon^n(x) &= -g_\varepsilon^n(x) + \beta_\varepsilon^n d_\varepsilon^{n-1}(x), \\ d_\mu^n(x) &= -g_\mu^n(x) + \beta_\mu^n d_\mu^{n-1}(x), \end{aligned}$$

with

$$\begin{aligned} \beta_\varepsilon^n &= \frac{\|g_\varepsilon^n(x)\|^2}{\|g_\varepsilon^{n-1}(x)\|^2}, \\ \beta_\mu^n &= \frac{\|g_\mu^n(x)\|^2}{\|g_\mu^{n-1}(x)\|^2}. \end{aligned}$$

Here, $d_\varepsilon^0(x) = -g_\varepsilon^0(x)$, $d_\mu^0(x) = -g_\mu^0(x)$ and $\alpha_\varepsilon, \alpha_\mu$ are step-sizes in the gradient update which can be computed as in [32].

- Step 3. Stop computing ε_h^n at the iteration $M := n$ and obtain the function $\varepsilon_h^M := \varepsilon_h^n$ if either $\|g_1^n\|_{L_2(\Omega)} \leq \theta$ or norms $\|\varepsilon_h^n\|_{L_2(\Omega)}$ are stabilized. Here, θ is the tolerance in n updates of the gradient method.
- Step 4. Stop computing μ_h^n at the iteration $N := n$ and obtain the function $\mu_h^N := \mu_h^n$ if either $\|g_2^n\|_{L_2(\Omega)} \leq \theta$ or norms $\|\mu_h^n\|_{L_2(\Omega)}$ are stabilized. Otherwise set $n := n + 1$ and go to step 1.

11.2 Adaptive algorithms

In this section we present two adaptive algorithms for the solution of our **IP**. In Adaptive algorithm 1 we apply first mesh refinement recommendation of Section 10, while in Adaptive algorithm 2 we use second mesh refinement recommendation of Section 10.

We define the minimizer of the Tikhonov functional (9) and its approximated finite element solution on k times adaptively refined mesh K_{h_k} by (ε, μ) and (ε_k, μ_k) , correspondingly. In our both mesh refinement recommendations of Section 10 we need compute the functions ε_k, μ_k on the mesh K_{h_k} . To do that we apply conjugate gradient algorithm of Section 11.1. We will define by $\varepsilon_k := \varepsilon_h^M, \mu_k := \mu_h^N$ values obtained at steps 3 and 4 of the conjugate gradient algorithm.

Adaptive Algorithm 1

- Step 0. Choose an initial space-time mesh $K_{h_0} \times J_{\tau_0}$ in $\Omega_{FEM} \times [0, T]$. Compute the sequences of $\varepsilon_k, \mu_k, k > 0$, via following steps:

Step 1. Obtain numerical solutions ε_k, μ_k on K_{h_k} using the Conjugate Gradient Method of Section 11.1.

Step 2. Refine such elements in the mesh K_{h_k} where the expression

$$|h\varepsilon_k| + |h\mu_k| \geq \tilde{\beta}_k \max_{\Omega_{FEM}} (|h\varepsilon_k| + |h\mu_k|) \quad (75)$$

is satisfied. Here, the tolerance numbers $\tilde{\beta}_k \in (0, 1)$ are chosen by the user.

Step 3. Define a new refined mesh as $K_{h_{k+1}}$ and construct a new time partition $J_{\tau_{k+1}}$ such that the CFL condition of [18] for explicit schemes (34) is satisfied. Interpolate ε_k, μ_k on a new mesh $K_{h_{k+1}}$ and perform steps 1-3 on the space-time mesh $K_{h_{k+1}} \times J_{\tau_{k+1}}$. Stop mesh refinements when $\|\varepsilon_k - \varepsilon_{k-1}\| < tol_1$ and $\|\mu_k - \mu_{k-1}\| < tol_2$ or $\|g_\varepsilon^k(x)\| < tol_3$ and $\|g_\mu^k(x)\| < tol_4$, where $tol_i, i = 1, \dots, 4$ are tolerances chosen by the user.

Adaptive Algorithm 2

Step 0. Choose an initial space-time mesh $K_{h_0} \times J_{\tau_0}$ in Ω_{FEM} . Compute the sequence $\varepsilon_k, \mu_k, k > 0$, on a refined meshes K_{h_k} via following steps:

Step 1. Obtain numerical solutions ε_k, μ_k on $K_{h_k} \times J_{\tau_k}$ using the Conjugate Gradient Method of Section 11.1.

Step 2. Refine the mesh K_{h_k} at all points where

$$|g_\varepsilon^k(x)| + |g_\mu^k(x)| \geq \beta_k \max_{\Omega} (|g_\varepsilon^k(x)| + |g_\mu^k(x)|), \quad (76)$$

where a posteriori error indicators g_ε^k, g_μ^k are defined in (71), (73). We choose the tolerance number $\beta_k \in (0, 1)$ in numerical examples.

Step 3. Define a new refined mesh as $K_{h_{k+1}}$ and construct a new time partition $J_{\tau_{k+1}}$ such that the CFL condition of [18] for explicit schemes (34) is satisfied. Interpolate ε_k, μ_k on a new mesh $K_{h_{k+1}}$ and perform steps 1-3 on the space-time mesh $K_{h_{k+1}} \times J_{\tau_{k+1}}$. Stop mesh refinements when $\|\varepsilon_k - \varepsilon_{k-1}\| < tol_1$ and $\|\mu_k - \mu_{k-1}\| < tol_2$ or $\|g_\varepsilon^k(x)\| < tol_3$ and $\|g_\mu^k(x)\| < tol_4$, where $tol_i, i = 1, \dots, 4$ are tolerances chosen by the user.

Remarks

- 1. First we make comments how to choose the tolerance numbers $\beta_k, \tilde{\beta}_k$ in (76), (75). Their values depend on the concrete values of $\max_{\Omega_{FEM}} (|g_\varepsilon^k(x)| + |g_\mu^k(x)|)$ and $\max_{\Omega_{FEM}} (|h\varepsilon_k| + |h\mu_k|)$, correspondingly. If we will take values of $\beta_k, \tilde{\beta}_k$ which are very close to 1 then we will refine the mesh in very narrow region of the Ω_{FEM} , and if we will choose $\beta_k, \tilde{\beta}_k \approx 0$ then almost all elements in the finite element mesh will be refined, and thus, we will get global and not local mesh refinement. Our numerical tests of Section 12 show that the choice of $\beta_k, \tilde{\beta}_k \equiv 0.7$ is almost optimal one since with these values of the parameters $\beta_k, \tilde{\beta}_k$ the finite element mesh K_h is refined exactly at the places where we have computed the functions (ε_h, μ_h) .
- 2. To compute L_2 norms $\|\varepsilon_k - \varepsilon_{k-1}\|, \|\mu_k - \mu_{k-1}\|$ in step 3 of adaptive algorithms the solutions $\varepsilon_{k-1}, \mu_{k-1}$ are interpolated from the mesh $K_{h_{k-1}}$ to the mesh K_{h_k} .

12 Numerical studies of the adaptivity technique

In this section we present numerical tests for solution of our **IP** using adaptive algorithm 1 of Section 11.2. Goal of our simulations is to show performance of the adaptivity technique in order to improve reconstruction which was obtained on a coarse non-refined mesh.

In our tests we reconstruct two symmetric structures of Figure 1 which represents model of a waveguide with small magnetic metallic inclusions with the relative permittivity $\varepsilon_r = 12$ and the relative magnetic permeability $\mu_r = 2.0$. We note that we choose in metallic targets $\varepsilon_r = 12$ similarly with our recent work [6] and experimental works [7, 8, 33] where metallic targets were treated as dielectrics with large dielectric constants and they were called *effective* dielectric constants. Values of them we choose similarly with [6, 7, 8, 33] in the interval

$$\varepsilon_r \in (10, 30). \quad (77)$$

In our tests we choose $\mu_r = 2.0$ because the relative magnetic permeability belongs to the interval $\mu_r \in [1, 3]$, see [36] and [6] for a similar choice.

As in [6] we initialize only one component E_2 of the electrical field $E = (E_1, E_2, E_3)$ on S_T as a plane wave $f(t)$ such that (see boundary condition in (6))

$$f(t) = \begin{cases} \sin(\omega t), & \text{if } t \in (0, \frac{2\pi}{\omega}), \\ 0, & \text{if } t > \frac{2\pi}{\omega}. \end{cases} \quad (78)$$

Compared with [6] where in computations only zero initial conditions in (6) were used, in Test 2 of our study we use non-zero initial condition for the second

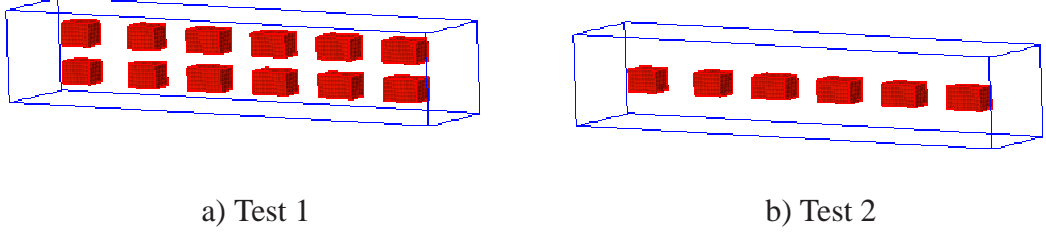


Figure 2: The exact values of functions $\varepsilon(x)$ and $\mu(x)$ are: $\varepsilon(x) = 12.0, \mu(x) = 2$ inside the small scatterers, and $\varepsilon(x) = \mu(x) = 1.0$ everywhere else in Ω_{FEM} .

component E_2 given by the function

$$\begin{aligned} f_0(x) &= E_2(x, 0) = \exp^{-(x_1^2+x_2^2+x_3^3)} \cdot \cos t|_{t=0} = \exp^{-(x_1^2+x_2^2+x_3^3)}, \\ f_1(x) &= \frac{\partial E_2}{\partial t}(x, 0) = -\exp^{-(x_1^2+x_2^2+x_3^3)} \cdot \sin t|_{t=0} \equiv 0. \end{aligned} \quad (79)$$

We perform two different tests with different inclusions to be reconstructed:

- Test 1. Reconstruction of two layers of scatterers of figure 2 -a) with additive noise $\sigma = 7\%$ and $\sigma = 17\%$ in backscattered data on the frequency interval for $\omega \in [45, 60]$ with zero initial conditions in (6).
- Test 2. Reconstruction of one layer of scatterers of figure 2-b) with additive noise $\sigma = 7\%$ and $\sigma = 17\%$ in backscattered data on the frequency interval for $\omega \in [45, 60]$ with one non-zero initial condition (79) in (6).

12.1 Computational domains

For simulations of forward and adjoint problems we use the domain decomposition method of [4]. This method is convenient for our computations since it is efficiently implemented in the software package WavES [40] using PETSc [37]. To apply method of [4] we divide our computational domain Ω into two subregions as described in Section 3, and we define $\Omega_{\text{FDM}} := \Omega_{\text{OUT}}$ such that $\Omega = \Omega_{\text{FEM}} \cup \Omega_{\text{FDM}}$, see Figure 1. In Ω_{FEM} we use finite elements and in Ω_{FDM} we will use finite difference method. We set functions $\varepsilon(x) = \mu(x) = 1$ in Ω_{FDM} and assume that they are unknown only in Ω_{FEM} . We choose the dimensionless domain Ω_{FEM} such that

$$\Omega_{\text{FEM}} = \{x' = (x_1, x_2, x_3) \in (-3.2, 3.2) \times (-0.6, 0.6) \times (-0.6, 0.6)\}.$$

and the dimensionless domain Ω is set to be

$$\Omega = \{x' = (x_1, x_2, x_3) \in (-3.4, 3.4) \times (-0.8, 0.8) \times (-0.8, 0.8)\}.$$

Here, the dimensionless spatial variable $x' = x / (1m)$. In the domain decomposition between Ω_{FEM} and Ω_{FDM} we choose the mesh size $h = 0.1$. We use also this mesh size for the coarse mesh K_{h_0} in both adaptive algorithms of Section 11.2. As in [4, 5, 6] in all our tests we set $s = 1$ in (??) in Ω_{FEM} .

Because of the domain decomposition the Maxwell's system (6) transforms to the wave equation in Ω_{FDM} such that

$$\begin{aligned} \frac{\partial^2 E}{\partial t^2} - \Delta E &= 0, \text{ in } \Omega_{FDM} \times [0, T], \\ E_2(x, 0) &= f_0(x), E_1(x, 0) = E_3(x, 0) = 0 \text{ for } x \in \Omega, \\ E_t(x, 0) &= 0 \text{ for } x \in \Omega, \\ E(x, t) &= (0, f(t), 0), \text{ on } \partial\Omega_1 \times (0, t_1], \\ \partial_n E(x, t) &= -\partial_t E(x, t), \text{ on } \partial\Omega_1 \times (t_1, T), \\ \partial_n E(x, t) &= -\partial_t E(x, t), \text{ on } \partial\Omega_2 \times (0, T), \\ \partial_n E(x, t) &= 0, \text{ on } \partial\Omega_3 \times (0, T). \end{aligned} \tag{80}$$

In Ω_{FEM} we solve

$$\begin{aligned} \varepsilon \frac{\partial^2 E}{\partial t^2} + \nabla \times (\mu^{-1} \nabla \times E) - s \nabla (\nabla \cdot (\varepsilon E)) &= 0, \text{ in } \Omega_{FEM}, \\ E(x, 0) = 0, \quad E_t(x, 0) &= 0 \text{ in } \Omega_{FEM}, \\ E(x, t)|_{\partial\Omega_{FEM}} &= E(x, t)|_{\partial\Omega_{FDM_I}}. \end{aligned} \tag{81}$$

In (81), $\partial\Omega_{FDM_I}$ denotes the internal boundary of the domain Ω_{FDM} , and $\partial\Omega_{FEM}$ denotes the boundary of the domain Ω_{FEM} . In a similar way transforms also the adjoint problem (18) into two problems in Ω_{FDM} and in Ω_{FEM} , which will be the same as in [6]. We solve the forward and adjoint problems in time $[0, T] = [0, 3]$ in both adaptive algorithms and choose the time step $\tau = 0.006$ which satisfies the CFL condition [18]. To be able test adaptive algorithms we first generate backscattered data at S_T by solving the forward problem (6) with the plane wave $f(t)$ given by (78) in the time interval $t = [0, 3]$ with $\tau = 0.006$ and with known values of $\varepsilon_r = 12.0, \mu_r = 2$ inside scatterers of Figure 2 and $\varepsilon_r = \mu_r = 1.0$ everywhere else in Ω . Figure 3 presents isosurfaces of the exact simulated solution at different times. Particularly, in Figure 3-c) we observe behaviour of non-zero initial condition (79). Our data were generated on a specially constructed mesh for the solution of the forward problem: this mesh was several times refined in the places where inclusions of Figure 2 are located. This mesh is completely different

than meshes used in computations in Tests 1, 2. Thus, the variational crime in our computations is avoided. Figures 4-a), b) illustrate typical behavior of noisy backscattered data in Test 1 running it with $\omega = 50$ in (78). Figure 4-b) shows result of computations of the forward problem in Test 2 when we take $\omega = 60$ in (78). Figure 4-c),d) show the difference in backscattered data for all components of the electrical field at final time of computations $t = 3$.

12.2 Reconstructions

Table 1. Results of reconstruction on a coarse meshes of Tables 5,6 for $\sigma = 7\%$ together with computational errors between $\max_{\Omega_{FEM}} \varepsilon_{\overline{N}}$ and exact ε^* in procents. Here, \overline{N} is the final iteration number in the conjugate gradient method for computation of ε_r , and \overline{M} is the final iteration number for computation of μ_r .

$\sigma = 7\%$						
Test 1	$\max_{\Omega_{FEM}} \varepsilon_{\overline{N}}$	error, %	\overline{N}	$\max_{\Omega_{FEM}} \mu_{\overline{M}}$	error, %	\overline{M}
$\omega = 45$	15	25	10	2.58	29	10
$\omega = 50$	15	25	10	2.38	19	10
$\omega = 60$	15	25	10	2.46	23	10
Test 2	$\max_{\Omega_{FEM}} \varepsilon_{\overline{N}}$	error, %	\overline{N}	$\max_{\Omega_{FEM}} \mu_{\overline{M}}$	error, %	\overline{M}
$\omega = 45$	13.32	11	10	3.07	53.5	10
$\omega = 50$	15	25	10	2.62	31	10
$\omega = 60$	9.3	22.4	10	2.88	44	10

Table 2. Results of reconstruction on a coarse meshes of Tables 5,6 for $\sigma = 17\%$ together with computational errors between $\max_{\Omega_{FEM}} \varepsilon_{\overline{N}}$ and exact ε^* in procents. Here, \overline{N} is the final iteration number in the conjugate gradient method for computation of ε_r , and \overline{M} is the final iteration number for computation of μ_r .

$\sigma = 17\%$						
Test 1	$\max_{\Omega_{FEM}} \varepsilon_{\overline{N}}$	error, %	\overline{N}	$\max_{\Omega_{FEM}} \mu_{\overline{M}}$	error, %	\overline{M}
$\omega = 45$	15	25	10	2.35	17.5	10
$\omega = 50$	15	25	10	2.89	44.5	10
$\omega = 60$	15	25	8	3.09	53.6	8
Test 2	$\max_{\Omega_{FEM}} \varepsilon_{\overline{N}}$	error, %	\overline{N}	$\max_{\Omega_{FEM}} \mu_{\overline{M}}$	error, %	\overline{M}
$\omega = 45$	15	25	10	2.39	19.5	10
$\omega = 50$	15	25	10	2.24	12	10
$\omega = 60$	8.46	29.5	10	2.50	25	10

Table 3. Results of reconstruction on a 5 times adaptively refined meshes of Tables 5,6 for $\sigma = 7\%$ together with computational errors between $\max_{\Omega_{FEM}} \varepsilon_{\overline{N}}$ and exact ε^* in percents. Here, \overline{N} is the final iteration number in the conjugate gradient method for computation of ε_r , and \overline{M} is the final iteration number for computation of μ_r .

$\sigma = 7\%$						
Test 1	$\max_{\Omega_{FEM}} \varepsilon_{\overline{N}}$	error, %	\overline{N}	$\max_{\Omega_{FEM}} \mu_{\overline{M}}$	error, %	\overline{M}
$\omega = 45$	14.96	24.6	3	1.82	9	3
$\omega = 50$	14.96	24.6	3	1.73	13.5	3
$\omega = 60$	14.95	24.5	3	1.76	12	3
Test 2	$\max_{\Omega_{FEM}} \varepsilon_{\overline{N}}$	error, %	\overline{N}	$\max_{\Omega_{FEM}} \mu_{\overline{M}}$	error, %	\overline{M}
$\omega = 45$	12.97	8	3	1.99	0.5	3
$\omega = 50$	14.57	21.4	3	1.79	10.5	3
$\omega = 60$	9.3	22.5	3	1.91	4.5	3

We start to run adaptive algorithms with guess values of $\varepsilon_r = 1.0, \mu_r = 1.0$ at all points in Ω . In our recent work [6] was shown that such choice of the initial guess gives a good reconstruction for both functions ε_r and μ_r , see also [2, 4] for a similar choice of initial guess for other coefficient inverse problems (CIPs). Taking into account (77) we choose following sets of admissible parameters for ε_r and μ_r

$$\begin{aligned} M_\varepsilon &\in \{\varepsilon \in C(\overline{\Omega}) | 1 \leq \varepsilon(x) \leq 15\}, \\ M_\mu &\in \{\mu \in C(\overline{\Omega}) | 1 \leq \mu(x) \leq 3\}. \end{aligned} \quad (82)$$

In our simulations we choose two constant regularization parameters $\gamma_1 = 0.01, \gamma_2 = 0.7$ in the Tikhonov functional (9). These parameters satisfy conditions (42) and were chosen because of our computational experience: such choices for the regularization parameters were optimal since they gave the smallest relative errors $e_\varepsilon = \frac{\|\varepsilon - \varepsilon_h\|}{\|\varepsilon_h\|}$ and $e_\mu = \frac{\|\mu - \mu_h\|}{\|\mu_h\|}$ in the reconstruction, see [6] for details. Iteratively regularized adaptive finite element method for our **IP** when zero initial conditions $f_0 = f_1 = 0$ in (6) are initialized, is recently presented in [34]. Currently we perform numerical experiments with iteratively regularized adaptive finite element method for the case when we initialize one non-zero initial condition (79) in (6). This work will be described in the forthcoming paper. In the above mentioned works iterative regularization is performed via algorithms of [2]. We also refer to [21, 26] for different techniques for the choice of regularization parameters.

To get our reconstructions of Figures 6 - 10, we use image post-processing procedure described in [6]. Tables 1-6 present computed results of reconstructions for ε_r and μ_r on different adaptively refined meshes after applying adaptive

Table 4. Results of reconstruction on a 5 times adaptively refined meshes of Tables 5,6 for $\sigma = 17\%$ together with computational errors between $\max_{\Omega_{FEM}} \varepsilon_{\overline{N}}$ and exact ε^* in percents. Here, \overline{N} is the final iteration number in the conjugate gradient method for computation of ε_r , and \overline{M} is the final iteration number for computation of μ_r .

$\sigma = 17\%$						
Test 1	$\max_{\Omega_{FEM}} \varepsilon_{\overline{N}}$	error, %	\overline{N}	$\max_{\Omega_{FEM}} \mu_{\overline{M}}$	error, %	\overline{M}
$\omega = 45$	14.96	24.6	3	1.65	17.5	3
$\omega = 50$	14.96	24.6	3	1.97	1.5	3
$\omega = 60$	14.95	24.5	3	2.04	20	3
Test 2	$\max_{\Omega_{FEM}} \varepsilon_{\overline{N}}$	error, %	\overline{N}	$\max_{\Omega_{FEM}} \mu_{\overline{M}}$	error, %	\overline{M}
$\omega = 45$	14.69	22.4	3	1.71	14.5	3
$\omega = 50$	14.47	20.5	3	1.63	18.5	3
$\omega = 60$	8.44	29.7	3	1.74	13	3

algorithm 1. Similar results are obtained for adaptive algorithm 2, and thus they are not presented here.

12.2.1 Test 1

In this example we performed simulations with two additive noise levels in data: $\sigma = 7\%$ and $\sigma = 17\%$, see Tables 1-6 for results. Using these tables we observe that the best reconstruction results for both noise levels are obtained for $\omega = 45$ in (78). Below we describe reconstructions obtained with $\omega = 45$ in (78) and $\sigma = 7\%$.

The reconstructions of ε_r and μ_r on initial coarse mesh are presented in Figure 5. Using Table 1 we observe that we achieve good values of contrast for both functions already on a coarse mesh. However, Figures 7-a), b) show us that the locations of all inclusions in x_3 direction should be improved. The reconstructions of ε_r and μ_r on a final adaptively refined mesh are presented in Figure 6. We observe significant improvement of reconstructions of ε_r and μ_r in x_3 direction on the final adaptively refined mesh compared with reconstructions obtained on a coarse mesh, see Figure 7. Figures 8-a), c), e) show different projections of final adaptively refined mesh which was used for computations of images of Figures 6, 7-c), d).

12.2.2 Test 2

In this test we again used two additive noise levels in data, $\sigma = 7\%$ and $\sigma = 17\%$, as well as non-zero initial condition (79) in (6). Results of computations

Table 5. Test 1. Computed values of $\varepsilon_r^{\text{comp}} := \max_{\Omega_{FEM}} \varepsilon_r$ and $\mu_r^{\text{comp}} := \max_{\Omega_{FEM}} \mu_r$ on the adaptively refined meshes. Computations are done with the noise $\sigma = 7\%$.

ω		coarse mesh	1 ref. mesh	2 ref. mesh	3 ref. mesh	4 ref. mesh	5 ref. mesh
45	# nodes	10958	11028	11241	11939	14123	18750
	# elements	55296	55554	56624	60396	73010	96934
	$\varepsilon_r^{\text{comp}}$	15	15	15	15	15	14.96
	μ_r^{comp}	2.58	2.58	2.58	2.58	2.58	1.82
50	# nodes	10958	11031	11212	11887	13761	17892
	# elements	55296	55572	56462	60146	71010	92056
	$\varepsilon_r^{\text{comp}}$	15	15	15	15	15	14.96
	μ_r^{comp}	2.38	2.38	2.38	2.38	2.38	1.73
60	# nodes	10958	11050	11255	11963	13904	18079
	# elements	55296	56666	60564	71892	61794	92926
	$\varepsilon_r^{\text{comp}}$	15	15	15	15	15	14.96
	μ_r^{comp}	2.46	2.46	2.46	2.46	2.46	1.76

Table 6. Test 2. Computed values of $\varepsilon_r^{\text{comp}} := \max_{\Omega_{FEM}} \varepsilon_r$ and $\mu_r^{\text{comp}} := \max_{\Omega_{FEM}} \mu_r$ on the adaptively refined meshes. Computations are done with the noise $\sigma = 17\%$.

ω		coarse mesh	1 ref. mesh	2 ref. mesh	3 ref. mesh	4 ref. mesh	5 ref. mesh
45	# nodes	10958	11007	11129	11598	12468	14614
	# elements	55428	55428	56024	58628	63708	74558
	$\varepsilon_r^{\text{comp}}$	15	15	15	15	15	14.96
	μ_r^{comp}	2.39	2.39	2.39	2.39	2.39	1.71
50	# nodes	10958	11002	11106	11527	12433	14494
	# elements	55296	55398	55908	58240	63540	73900
	$\varepsilon_r^{\text{comp}}$	15	15	15	15	15	14.47
	μ_r^{comp}	2.24	2.24	2.24	2.24	2.24	1.63
60	# nodes	10958	11002	11104	11560	12459	14888
	# elements	55296	55398	55904	58402	63628	76068
	$\varepsilon_r^{\text{comp}}$	8.46	8.46	8.46	8.46	8.46	8.44
	μ_r^{comp}	2.50	2.50	2.50	2.50	2.50	1.74

are presented in Tables 1-6. Using these tables we see that the best reconstruction results in this test for both noise levels are obtained for $\omega = 50$ in (78). We now describe reconstructions obtained for $\omega = 50$ in (78) and $\sigma = 17\%$.

The reconstructions of ε_r and μ_r on a coarse mesh are shown in Figure 9. The reconstructions of ε_r and μ_r on a final adaptively refined mesh are given in Figure 10. We again observe significant improvement of reconstructions of ε_r and μ_r in x_3 direction on the final adaptively refined mesh in comparison to the reconstruction obtained on a coarse mesh, see Figure 11. Figures 8-b), d), f) show different projections of final adaptively refined mesh which was used for computations of images of Figures 10, 11-c),d).

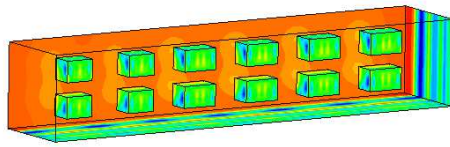
13 Conclusion

This work is a continuation of our previous study in [6] and is focused on the solution of coefficient inverse problem for simultaneously reconstruction of functions ε and μ from time-dependent backscattered data in the Maxwell's equations. To do that we have used optimization approach of [6] applied on adaptively refined meshes.

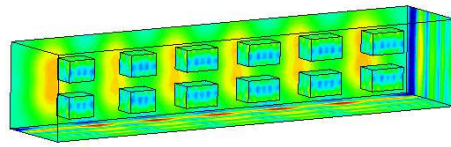
We derived a posteriori error estimates in the reconstructed coefficients ε and μ and in the Tikhonov functional to be minimized. We then formulated two adaptive algorithms which allow reconstruction of ε and μ on the locally adaptively refined meshes using these estimates.

Numerically we tested our algorithms with two different noise levels, $\sigma = 7\%$ and $\sigma = 17\%$, on the frequency band $\omega \in [45, 60]$. Main conclusion of our previous study of [6] was that we could get the large contrast of the dielectric function ε_r which allows us to reconstruct metallic targets, and that the contrast for μ_r was within limits of (82). However, the size of μ_r in x_1, x_2 directions and location of all inclusions in x_3 direction should be improved. Using Figures 5, 9 and Tables 1-6 of this note we can conclude that on the coarse mesh we get similar results as were obtained in [6]. However, with mesh refinements, as was expected, quality of reconstruction is improved a lot, see Figures 7, 10, 11. Using these Figures and Tables 1-6 we observe that now all inclusions have correct locations in x_3 direction as well as their contrasts and sizes in x_1, x_2 directions are also improved and reconstructed with a good accuracy. We can conclude, that we have supported tests of our previous works [3, 5, 7, 10, 29] and have shown that the adaptive finite element method is very powerful tool for the reconstruction of heterogeneous targets, their locations and shapes accurately.

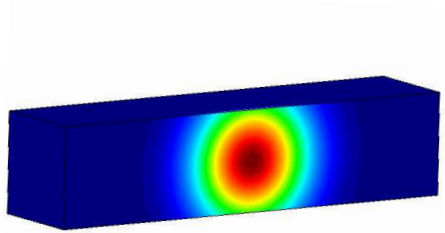
Our adaptive algorithms can also be applied for the case when edge elements are used for the numerical simulation of the solutions of forward and adjoint problems, see [16, 17, 23] for finite element analysis in this case. This as well as



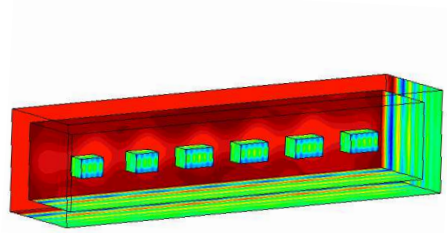
a) FEM solution at $t = 1.5$



b) FEM solution at $t = 1.8$



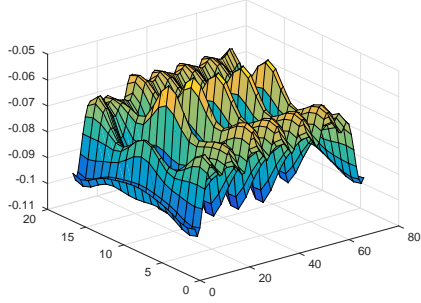
c) FEM/FDM solution at $t = 0$



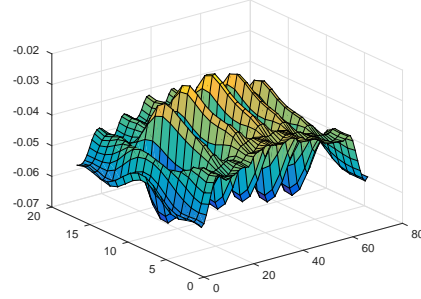
d) FEM/FDM solution at $t = 1.8$

Figure 3: Isosurfaces of the simulated FEM/FDM solution of the model problem at different times: a), b) Test 1; c), d) Test 2.

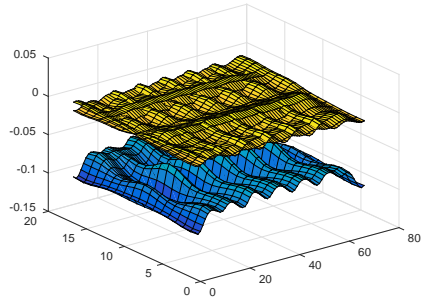
development of iteratively regularized adaptive finite element method can be considered as a challenge for the future research.



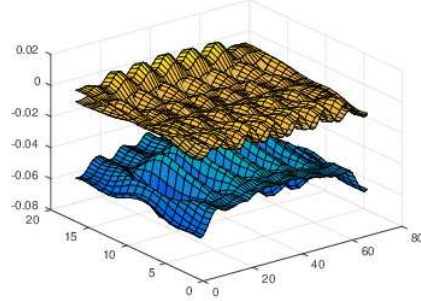
(a) Test 1. $\omega = 50, \sigma = 7\%, t = 3$



(b) Test 2. $\omega = 60, \sigma = 17\%, t = 3$

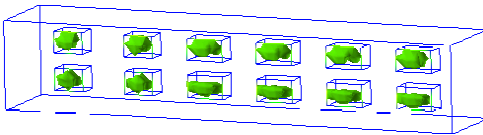


(c) Test 1. $\omega = 50, \sigma = 7\%, t = 3$

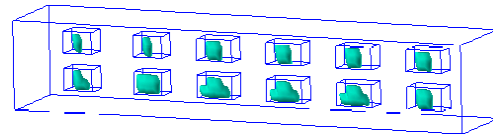


(d) Test 2. $\omega = 60, \sigma = 17\%, t = 3$

Figure 4: a), b) Backscattered data of the one component, $E_2(x, t)$, of the electric field $E(\mathbf{x}, t)$. c), d) Computed components E_2 (below) and E_1 and E_3 (on top) of the backscattered electric field $E(\mathbf{x}, t)$.



(a) $\max_{\Omega_{FEM}} \varepsilon_r \approx 15$



(b) $\max_{\Omega_{FEM}} \mu_r \approx 2.5$

Figure 5: Test 1. Computed images of reconstructed functions $\varepsilon_r(\mathbf{x})$ and $\mu_r(\mathbf{x})$ on a coarse mesh for $\omega = 45, \sigma = 7\%$.

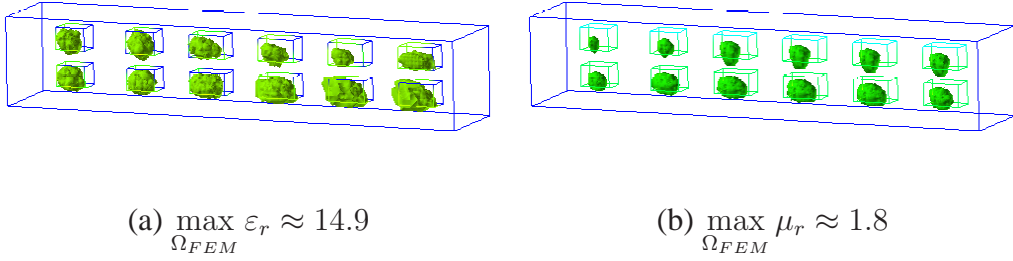


Figure 6: Test 1. Computed images of reconstructed functions $\varepsilon_r(\mathbf{x})$ and $\mu_r(\mathbf{x})$ on a 5 times adaptively refined mesh presented in Figure 8. Computations are done for $\omega = 45, \sigma = 7\%$.

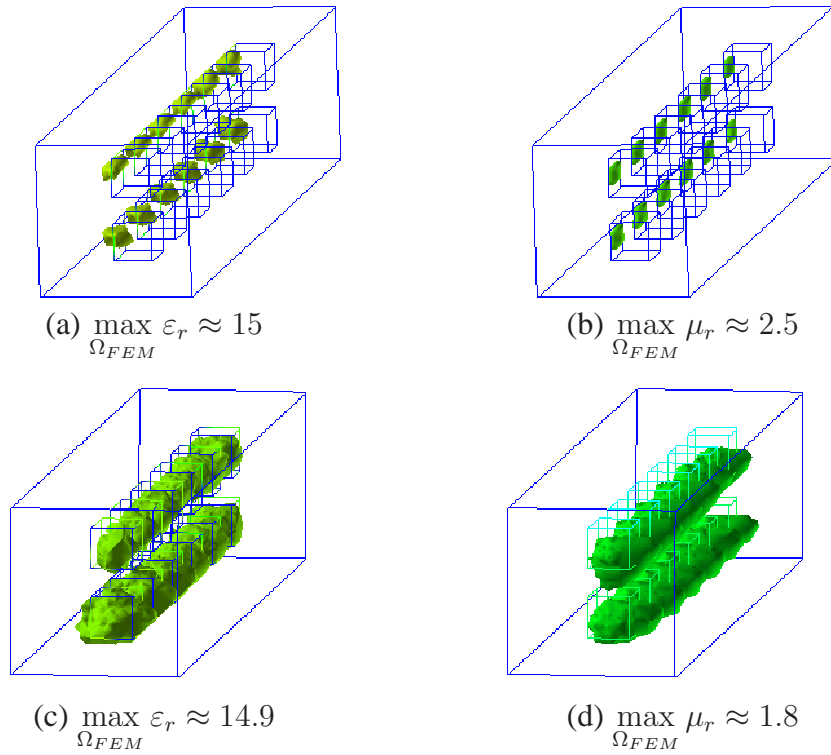


Figure 7: Test 1. Computed images of reconstructed functions $\varepsilon_r(\mathbf{x})$ and $\mu_r(\mathbf{x})$ in x_2x_3 view: a), b) on a coarse mesh, c), d) on a 5 times adaptively refined mesh. Computations are done for $\omega = 45, \sigma = 7\%$.

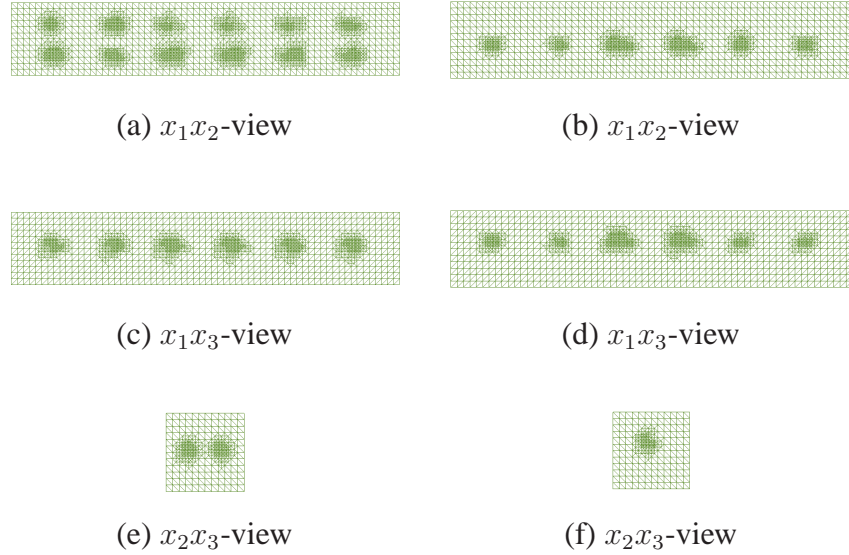


Figure 8: Different projections of 5 times adaptively refined meshes for computed images of Figures 6 (on the left) and Figures 10 (on the right), respectively.

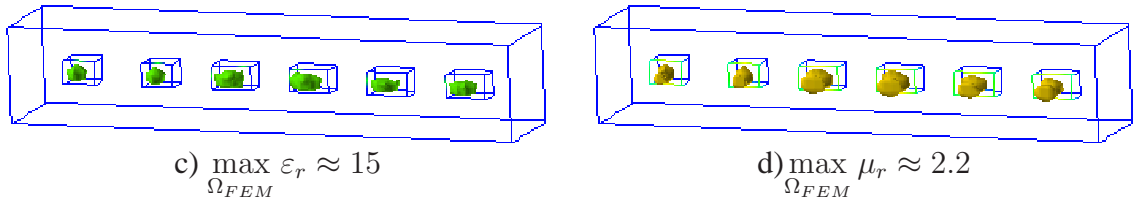


Figure 9: Test 2. Computed images of reconstructed functions $\varepsilon_r(\mathbf{x})$ and $\mu_r(\mathbf{x})$ on a coarse mesh for $\omega = 50$, $\sigma = 17\%$.

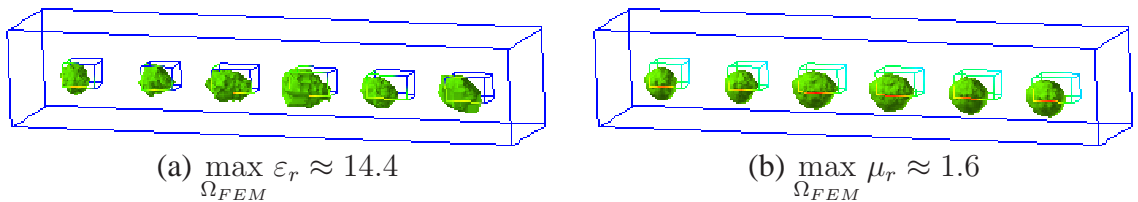
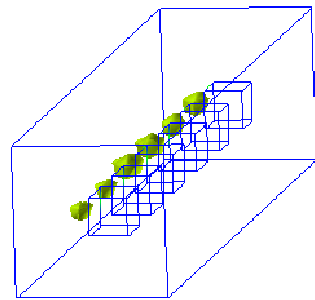
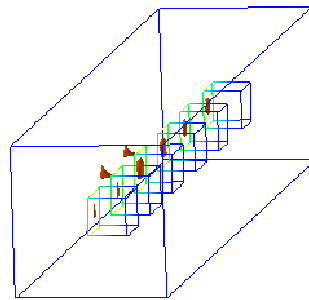


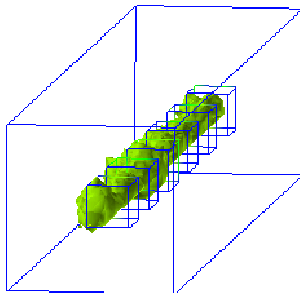
Figure 10: Test 2. Computed images of reconstructed functions $\varepsilon_r(\mathbf{x})$ and $\mu_r(\mathbf{x})$ on a 5 times adaptively refined mesh. Computations are done with $\omega = 50$, $\sigma = 17\%$.



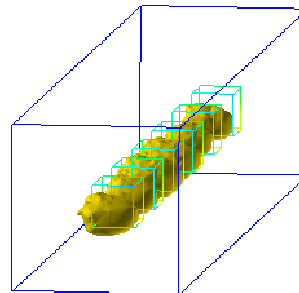
(a) $\max_{\Omega_{FEM}} \varepsilon_r \approx 15$



(b) $\max_{\Omega_{FEM}} \mu_r \approx 2.2$



(a) $\max_{\Omega_{FEM}} \varepsilon_r \approx 14.4$



(b) $\max_{\Omega_{FEM}} \mu_r \approx 1.6$

Figure 11: Test 2. Computed images of reconstructed functions $\varepsilon_r(\mathbf{x})$ and $\mu_r(\mathbf{x})$ in x_2x_3 view: a), b) on a coarse mesh, c), d) on a 5 times adaptively refined mesh. Computations are done for $\omega = 50$, $\sigma = 17\%$.

Acknowledgments

This research is supported by the Swedish Research Council (VR). The computations were performed on resources at Chalmers Centre for Computational Science and Engineering (C3SE) provided by the Swedish National Infrastructure for Computing (SNIC).

References

- [1] F. Assous, P. Degond, E. Heintze and P. Raviart, On a finite-element method for solving the three-dimensional Maxwell equations, *Journal of Computational Physics*, **109** (1993), 222–237.
- [2] A. Bakushinsky, M. Y. Kokurin, A. Smirnova, *Iterative Methods for Ill-posed Problems*, Inverse and Ill-Posed Problems Series 54, De Gruyter, 2011.
- [3] L. Beilina and C. Johnson, A posteriori error estimation in computational inverse scattering, *Mathematical Models in Applied Sciences*, **1** (2005), 23-35.
- [4] L. Beilina, Energy estimates and numerical verification of the stabilized Domain Decomposition Finite Element/Finite Difference approach for time-dependent Maxwell's system, *Central European Journal of Mathematics*, **11** (2013), 702-733 DOI: 10.2478/s11533-013-0202-3.
- [5] L. Beilina, Adaptive Finite Element Method for a coefficient inverse problem for the Maxwell's system, *Applicable Analysis*, **90** (2011) 1461-1479.
- [6] L. Beilina, M. Cristofol and K. Niinimäki, Optimization approach for the simultaneous reconstruction of the dielectric permittivity and magnetic permeability functions from limited observations, *Inverse Problems and Imaging*, 9 (1), pp. 1-25, 2015
- [7] L. Beilina, N. T. Thành, M. V. Klibanov, J. Bondestam-Malmberg, Reconstruction of shapes and refractive indices from blind backscattering experimental data using the adaptivity, *Inverse Problems*, **30**, 105007, 2014.
- [8] L. Beilina, N. T. Thành, M. V. Klibanov, M. A. Fiddy, Reconstruction from blind experimental data for an inverse problem for a hyperbolic equation, *Inverse Problems*, **30** (2014), 025002.

- [9] L. Beilina, M.V. Klibanov, *Approximate global convergence and adaptivity for coefficient inverse problems*, Springer, New-York, 2012.
- [10] L. Beilina, M.V. Klibanov and M.Yu. Kokurin, Adaptivity with relaxation for ill-posed problems and global convergence for a coefficient inverse problem, *Journal of Mathematical Sciences*, 167, pp. 279-325, 2010.
- [11] L. Beilina, M. Grote, Adaptive Hybrid Finite Element/Difference Method for Maxwell's equations, *TWMS Journal of Pure and Applied Mathematics*, V.1(2), pp.176-197, 2010.
- [12] M. Bellassoued, M. Cristofol, and E. Soccorsi, Inverse boundary value problem for the dynamical heterogeneous Maxwell's system, *Inverse Problems*, (28), 095009, 2012.
- [13] J. Bondestam Malmberg, A posteriori error estimate in the Lagrangian setting for an inverse problem based on a new formulation of Maxwell's system, *Inverse Problems and Applications, Springer Proceedings in Mathematics and Statistics*, Vol. 120, 2015, pp. 42-53, 2015.
- [14] J. Bondestam Malmberg, A posteriori error estimation in a finite element method for reconstruction of dielectric permittivity, arXiv:1502.07658, 2015.
- [15] S. C. Brenner and L. R. Scott, *The Mathematical Theory of Finite Element Methods* (2nd edn), Springer-Verlag, New York, 2002.
- [16] P. Ciarlet, Jr. and J. Zou, Fully discrete finite element approaches for time-dependent Maxwell's equations, *Numerische Mathematik* **82** (1999), 193-219.
- [17] P. Ciarlet, Jr., H. Wu and J. Zou, Edge element methods for Maxwell's equations with strong convergence for Gauss' laws, *SIAM Journal on Numerical Analysis* **52** (2014), 779-807.
- [18] R. Courant, K. Friedrichs and H. Lewy On the partial differential equations of mathematical physics, *IBM Journal of Research and Development*, **11** (1967), 215-234.
- [19] G. C. Cohen, *Higher order numerical methods for transient wave equations*, Springer-Verlag, 2002.
- [20] A. Elmkies and P. Joly, Finite elements and mass lumping for Maxwell's equations: the 2D case. *Numerical Analysis*, **324** (1997), 1287-1293.

- [21] H. W. Engl, M. Hanke and A. Neubauer, *Regularization of Inverse Problems* Boston: Kluwer Academic Publishers, 2000.
- [22] B. Engquist and A. Majda, Absorbing boundary conditions for the numerical simulation of waves, *Mathematics of Computation*, **31** (1977), 629-651.
- [23] H. Feng, D. Jiang and J. Zou, Simultaneous identification of electric permittivity and magnetic permeability, *Inverse Problems*, **26** (2010), 095009.
- [24] D. W. Einters, J. D. Shea, P. Komar, B. D. Van Veen and S. C. Hagness Three-dimensional microwave breast imaging: Dispersive dielectric properties estimation using patient-specific basis functions *IEEE Transactions on Medical Imaging* **28** (2009), 969–981
- [25] K. Eriksson, D. Estep and C. Johnson, *Calculus in Several Dimensions*, Springer, Berlin, 2004.
- [26] K Ito, B Jin, and T Takeuchi Multi-parameter Tikhonov regularization, *Methods and Applications of Analysis*, **18** (2011), 31–46.
- [27] C. Johnson and A. Szepessy, Adaptive finite element methods for conservation laws based on a posteriori error estimation, *Comm. Pure Appl. Math.*, 48, 199–234, 1995.
- [28] C. Johnson, *Numerical Solution of Partial Differential Equations by the Finite Element Method*, Dover Books on Mathematics, 2009.
- [29] M.V. Klibanov, A.B. Bakushinsky and L. Beilina, Why a minimizer of the Tikhonov functional is closer to the exact solution than the first guess, *J. Inverse and Ill-Posed Problems*, 19, 83-105, 2011.
- [30] O. A. Ladyzhenskaya, *Boundary Value Problems of Mathematical Physics*, Springer Verlag, Berlin, 1985.
- [31] C. D. Munz, P. Omnes, R. Schneider, E. Sonnendrucker and U. Voss, Divergence correction techniques for Maxwell Solvers based on a hyperbolic model, *Journal of Computational Physics*, **161** (2000), 484–511.
- [32] O. Pironneau, *Optimal shape design for elliptic systems*, Springer-Verlag, Berlin, 1984.

- [33] N. T. Thành, L. Beilina, M. V. Klibanov, M. A. Fiddy, Reconstruction of the refractive index from experimental backscattering data using a globally convergent inverse method, *SIAM J. Scientific Computing*, 36 (3) (2014), 273-293.
- [34] S. Hosseinzadegan, Iteratively regularized adaptive finite element method for reconstruction of coefficients in Maxwell's system, *Master's Thesis in Applied Mathematics*, Department of Mathematical Sciences, Chalmers University of Technology and Gothenburg University, 2015.
- [35] L. R. Scott, S. Zhang, Finite element interpolation of nonsmooth functions satisfying boundary conditions, *Math. Comp.*, **54** (1990), 483–493.
- [36] D. R. Smith, S. Schultz, P. Markos and C. M. Soukoulis, Determination of effective permittivity and permeability of metamaterials from reflection and transmission coefficients, *Physical Review B*, **65** (2002), DOI:10.1103/PhysRevB.65.195104.
- [37] PETSc, Portable, Extensible Toolkit for Scientific Computation, <http://www.mcs.anl.gov/petsc/>.
- [38] A.N. Tikhonov, A.V. Goncharsky, V.V. Stepanov and A.G. Yagola, *Numerical Methods for the Solution of Ill-Posed Problems*, London: Kluwer, London, 1995.
- [39] Tikhonov A.N., Goncharskiy A.V., Stepanov V.V., Kochikov I.V. Ill-posed problems of the image processing, DAN USSR, 294, 4. 832-837, 1987.
- [40] WavES, the software package, <http://www.waves24.com>
- [41] X. Zhang, H. Tortel, S. Ruy and A. Litman Microwave imaging of soil water diffusion using the linear sampling method, *IEEE Geoscience and Remote Sensing Letters* **8** (2011), 421–425